JOURNAL OF PETROLOGY | VOLUME 46 | NUMBER 3 | PAGES 615–639 | 2005 | doi:10.1093/petrology/egh091

REE and PGE Geochemical Constraints on the Formation of Dunites in the Luobusa Ophiolite, Southern Tibet

MEI-FU ZHOU[1]*, PAUL T. ROBINSON[1], JOHN MALPAS[1], STEPHEN J. EDWARDS[2] AND LIANG QI[1]

[1]DEPARTMENT OF EARTH SCIENCES, UNIVERSITY OF HONG KONG, POKFULAM ROAD, HONG KONG, CHINA

[2]DEPARTMENT OF EARTH AND ENVIRONMENTAL SCIENCES, UNIVERSITY OF GREENWICH AT MEDWAY, CHATHAM MARITIME ME4 4TB, UK

RECEIVED OCTOBER 20, 2003; ACCEPTED OCTOBER 18, 2004
ADVANCE ACCESS PUBLICATION DECEMBER 3, 2004

The Luobusa ophiolite, Southern Tibet, lies in the Indus–Yarlung Zangbo suture zone that separates Eurasia to the north from the Indian continent to the south. The ophiolite contains a well-preserved mantle sequence consisting of harzburgite, clinopyroxene (cpx)-bearing harzburgite and dunite. The harzburgite contains abundant pods of chromitite, most of which have dunite envelopes, and the cpx-bearing harzburgites host numerous dunite dykes. Dunite also exists as a massive unit similar to those of the mantle–crust transition zones in other ophiolites. All of the dunites in the ophiolite have a similar mineralogy, comprising mainly olivine with minor orthopyroxene and chromite and traces of clinopyroxene. They also display similar chemical compositions, including U-shaped chondrite-normalized REE patterns. Mantle-normalized PGE patterns show variable negative Pt anomalies. Detailed analysis of a chromite-bearing dunite dyke, which grades into the host cpx-bearing harzburgite, indicates that LREE and Ir decrease, whereas HREE, Pd and Pt increase away from the dunite. These features are consistent with formation of the dunite dykes by interaction of MORB peridotites with boninitic melts from which the chromitites were formed. Because the transition-zone dunites are mineralogically and chemically identical to those formed by such melt–rock reaction, we infer that they are of similar origin. The Luobusa ultramafic rocks originally formed as MORB-source upper mantle, which was subsequently trapped as part of a mantle wedge above a subduction zone. Hydrous melts generated under the influence of the subducted slab at depth migrated upward and reacted with the cpx-bearing harzburgites to form the dunite dykes. The modified melts ponded in small pockets higher in the section, where they produced podiform chromitites with dunite envelopes. At the top of the mantle section, pervasive reaction between melts and harzburgite produced the transition-zone dunites.

KEY WORDS: *melt–rock interaction; REE; PGE; hydrous melt; mantle; ophiolite; Tibet*

INTRODUCTION

Investigations of the geochemistry and petrology of ophiolitic peridotites provide constraints on processes such as partial melting, melt–rock interaction and melt fractionation that control the evolution of the uppermost mantle and aspects of the overlying crust (e.g. Coleman, 1977; Suen *et al.*, 1979; Nicolas & Prinzhofer, 1983; Kelemen *et al.*, 1992, 1995; Parkinson & Pearce, 1998; Godard *et al.*, 2000; Takazawa *et al.*, 2003). One of the more fruitful lines of study, particularly for understanding the processes of melt generation and modification in the mantle, and subsequent melt extraction, has been that of the relationships among dunite–pyroxenite veins and dykes, dunite lenses, podiform chromitites and their host tectonized peridotites (Malpas, 1978; Quick, 1981; Edwards, 1990; Edwards & Malpas, 1996; Zhou *et al.*, 1996; Suhr *et al.*, 1998, 2003; Kubo, 2002).

In ophiolites, dunites occur in a number of settings: (1) they are found throughout the mantle tectonites, interbanded with more pyroxene-rich peridotites; (2) they occur as discordant veins and dykes, a few centimetres

*Corresponding author. Telephone: (852) 2857 8251. Fax: (852) 2517 6712. E-mail: MFZHOU@hkucc.hku.hk

to several metres thick, which may or may not have accessory chromite and/or pyroxene; (3) they exist as larger discordant bodies, commonly with lensoid shapes, which have generally gradational contacts with their host peridotite; (4) they form envelopes or rinds around podiform chromitites; (5) they commonly form large masses in the transition zone between the mantle tectonites and the overlying layered plutonic sequence, i.e. at the mantle–crust boundary. The 'transition-zone dunites' are usually a few tens to hundreds of metres thick, show gradational or sharp contacts with the underlying mantle harzburgites, and have upper contacts marked by increasing amounts of plagioclase as they grade into layered troctolite and olivine gabbro of the crustal section.

The origin of the various dunite bodies, particularly the transition-zone dunites, has long been debated. Several workers have proposed that they are essentially magmatic, formed by olivine accumulation from a picritic magma (e.g. Coleman, 1977; Malpas, 1978; Pallister & Hopson, 1981; Quick, 1981). Certainly, the extent and thickness of some transition-zone dunites and their location at the base of a layered ultramafic and gabbroic section of the crust are supportive of a cumulate origin. Others have suggested that at least some dunite veins, dykes and smaller discordant bodies have a residual origin, formed either as remnants of advanced partial melting of lherzolite or harzburgite or by melt–rock interaction (Arai, 1980; Nicolas & Prinzhofer, 1983; Kelemen *et al.*, 1995; Zhou *et al.*, 1996).

Clearly, ophiolitic dunites are formed by a variety of complex, multi-stage processes. One way to unravel the resulting complexity and to constrain the origin of dunite is to perform detailed, small-scale studies of harzburgite–dunite transitions. In a preliminary study of the Luobusa ophiolite, Southern Tibet, Zhou *et al.* (1996) reported a dramatic change in chromite composition across a dunite envelope formed by melt–rock reaction between boninitic liquids and the host harzburgite, but detailed geochemical data were not available.

In this paper, we attempt to characterize various igneous processes occurring in the Luobusa mantle by examining the geochemistry of rare earth elements (REE) and platinum group elements (PGE), both of which are known to be sensitive indicators of processes such as partial melting, melt–rock interaction and magmatic fractionation (e.g. Quick, 1981; Edwards, 1990; Kelemen *et al.*, 1992; Prichard & Lord, 1993; Zhou *et al.*, 1996; Suhr *et al.*, 1998, 2003; Kubo, 2002). Only a few integrated studies relating the behaviour of REE and PGE to dunite and chromitite formation are available in the literature (Proenza *et al.*, 1999; Buchl *et al.*, 2002), and the importance of these elements in unravelling mantle processes is, to date, poorly understood. In Luobusa, we have undertaken a detailed study of the entire mantle sequence and of a small-scale melt–rock reaction zone. Here, we provide new geochemical data, including major oxides, Ni, Cu, REE, and PGE, and use these data to investigate the origin of dunites in the mantle section.

GEOLOGICAL BACKGROUND

The Luobusa ophiolite is located about 200 km east-south-east of Lhasa in the Indus–Yarlung Zangbo suture zone that separates the Lhasa Block to the north from the Indian continent to the south. It is a fault-bounded slab, approximately 1–2 km thick, which has been thrust northward onto Tertiary molasse deposits of the Luobusa Formation and the Gangdese batholith (Aitchison *et al.*, 2003) (Fig. 1). At the base of the ophiolite is a mélange zone containing lenses of pillow lava and cumulate rocks, including wehrlite, pyroxenite and layered and varitextured gabbro in a serpentinite matrix. Structurally, the ophiolite consists of several inverted thrust slices, such that the 'pseudostratigraphy' is upside-down (Fig. 1). In the reconstructed section, the deepest rocks are clinopyroxene-bearing harzburgites that contain numerous dunite dykes, some of which contain stringers (Fig. 2a) or bands of chromite (Fig. 2b). The overlying harzburgites contain abundant pods of chromitite, most of which have well-developed dunite envelopes (Zhou *et al.*, 1996). At the top of the mantle sequence is a massive, transition-zone dunite, a few metres to 300 m thick. The boundary between the transition-zone dunite and harzburgite is relatively sharp, whereas that between the harzburgite and cpx-bearing harzburgite is gradational.

The ophiolite is believed to have formed in two stages. Stage 1 is represented by MORB-source mantle and gabbroic dykes, whereas stage 2 is marked by the intrusion of boninitic melts from which the chromitites were precipitated (Malpas *et al.*, 2003). The Sm–Nd isochron for two whole rocks and plagioclase and clinopyroxene separates from one of the gabbroic dykes yielded an age of 177 ± 31 Ma (Zhou *et al.*, 2002). The Nd- and Pb-isotopic characteristics of the dyke have a Tethyan Ocean affinity, suggesting formation of the ophiolite in an oceanic setting during the Middle Jurassic (Zhou *et al.*, 2002). A zircon SHRIMP date of 126 Ma has been obtained from the Xigaze ophiolite further west in the belt, which also has a suprasubduction zone affinity, suggesting a Cretaceous age for the second stage of formation (Malpas *et al.*, 2003). Ar–Ar dates on amphibolites from the mélange zone range from 90 to 80 Ma and are interpreted as the age of intra-oceanic thrusting (Aitchison *et al.*, 2000; Malpas *et al.*, 2003). Final exhumation and emplacement probably took place in the Early Neogene (Malpas *et al.*, 2003).

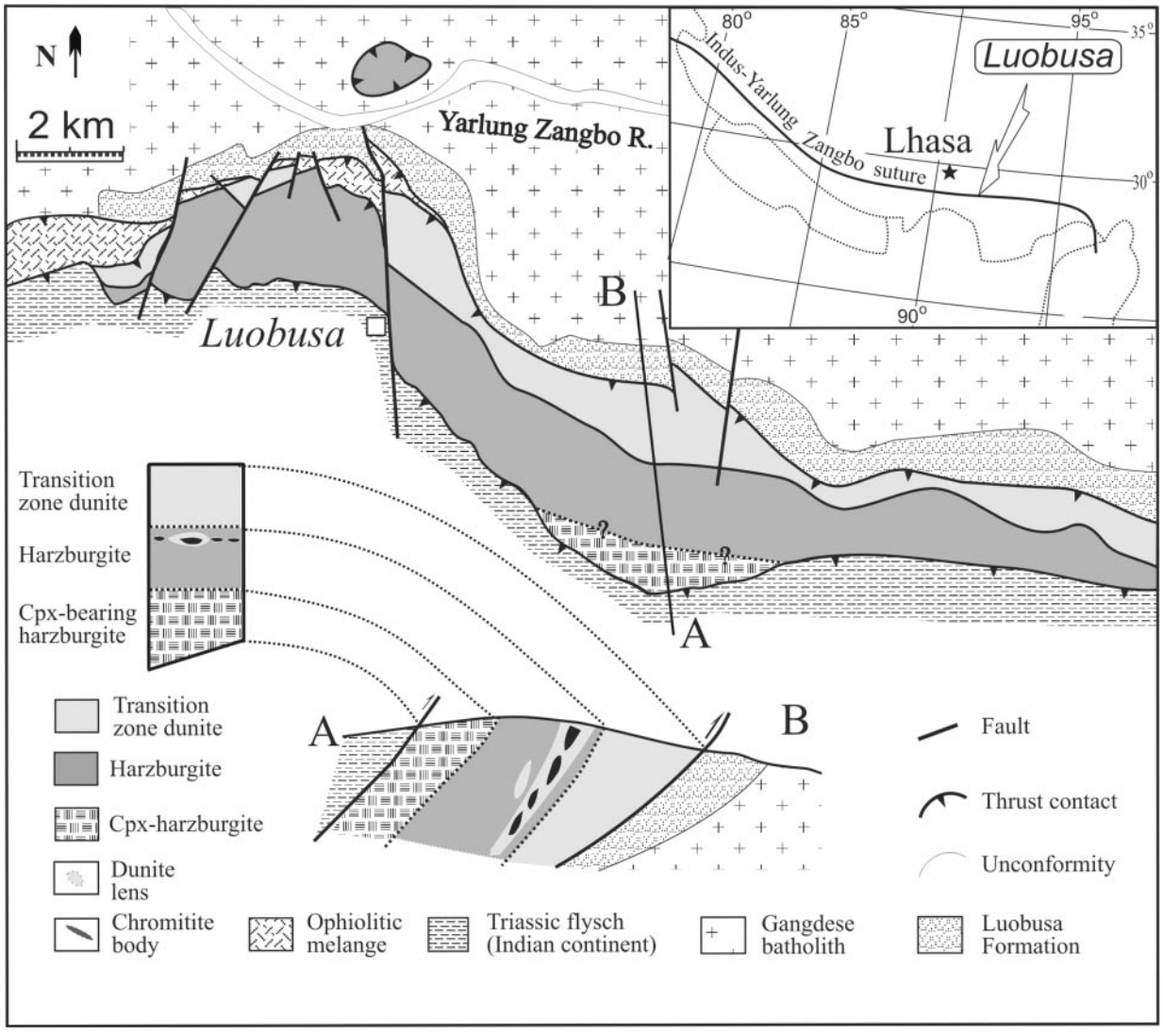

Fig. 1. Geological map of the Luobusa ophiolite, Southern Tibet (modified after Zhou *et al.*, 1996; Malpas *et al.*, 2003), showing a restored vertical section and a cross-section along the sampling traverse.

PETROGRAPHY

Harzburgite

The harzburgites display porphyritic textures with large (1–3 cm) subhedral orthopyroxene grains surrounded by smaller grains of olivine and sparse chromite (Fig. 3a). The least depleted varieties (cpx-bearing harzburgite) also contain 2–4 modal% of small (0·5–1 mm), anhedral clinopyroxene grains. Both olivine and orthopyroxene show internal deformation, but the rocks do not have a strong foliation. Olivine displays deformation lamellae along its slip planes, mini-kinking and irregular, extinction band configurations. The orthopyroxene slip system involves exsolution along the slip planes, kink band development and dynamic recrystallization. Both olivine and pyroxene have been granulated along microshears and grain boundaries and have locally undergone dynamic recrystallization (Zhou, 1995). Most of the accessory chromite is amoeboid in shape and ranges up to 1·5 mm across, but some occurs as tiny, scattered, interstitial grains at triple junctions of olivine crystals or enclosed in olivine and orthopyroxene. Both the harzburgites and cpx-bearing harzburgites are typically fresh with only sparse veinlets filled with talc and serpentine. A few samples show somewhat more extensive alteration along fractures and grain boundaries.

Transition-zone dunite

Transition-zone dunites consist chiefly of olivine with minor chromite and sparse interstitial orthopyroxene and diopside (Fig. 3b). Olivine grains are coarse- to very

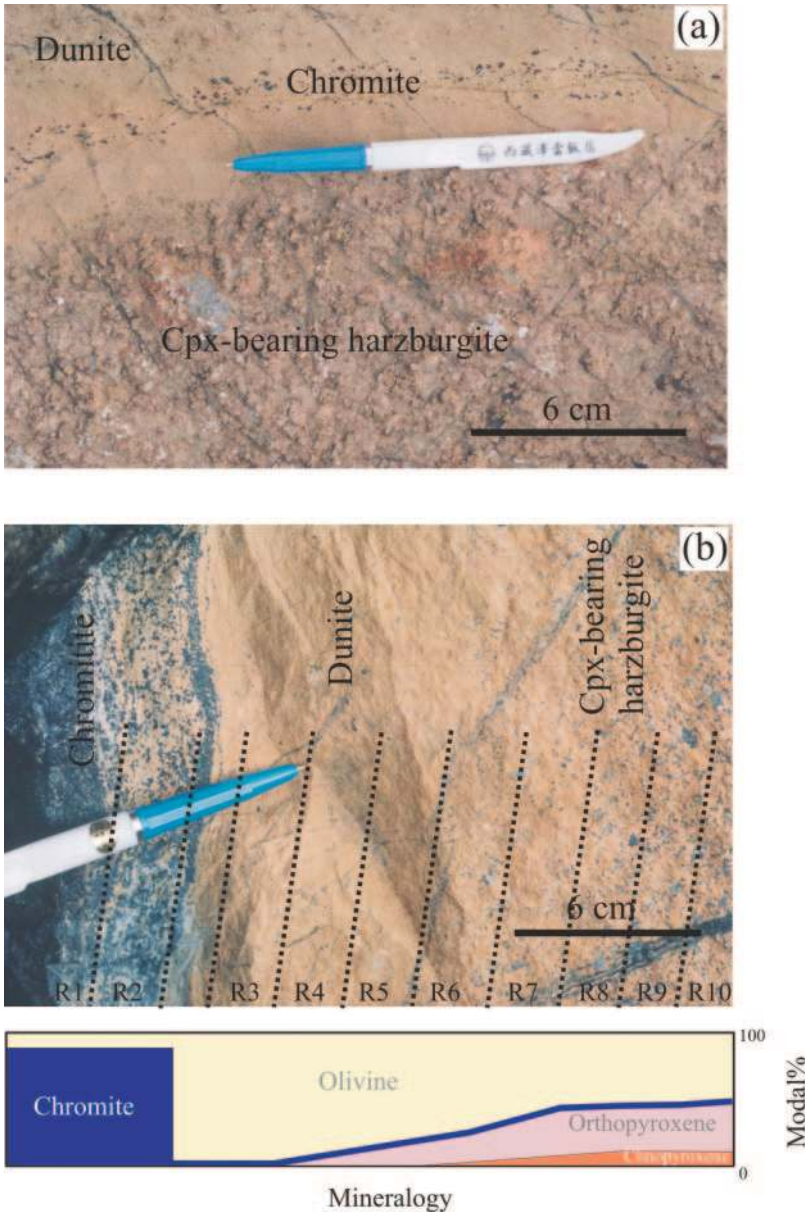

Fig. 2. Field photographs of dunite dykes in cpx-bearing harzburgite. (a) A dyke with a narrow band of chromite and a narrow transition zone between cpx-bearing harzburgite and dunite; (b) transition reaction zone around a dunite dyke containing a well-developed chromitite band. Note the decreasing modal percent of pyroxene in the transition zone. Ten samples (R1–10) were taken at 2 cm intervals across the reaction zone (see Table 3).

coarse-grained (up to a few centimetres) and most are elongated, giving the rock a crude foliation (Fig. 3c and d). Most of the dunites are cut by narrow shear zones filled with olivine neoblasts 0·05–0·1 mm across (Fig. 3d and e). Some of the neoblasts are elongated but others exhibit well-developed granoblastic textures with 120° grain boundary intersections, indicating annealing after deformation ceased (Fig. 3f). Exaggerated grain growth of olivine 'porphyroblasts' over chromite foliations or chromite layering, and smoothly curved boundaries between coarse-grained olivine–olivine and olivine–orthopyroxene crystal pairs, are also common in the dunites.

Most of the dunites are very fresh, with only minor serpentine and talc along narrow veinlets, less than 1 mm wide. Increasing degrees of alteration are marked by growth of secondary minerals along cracks and grain boundaries, leading eventually to small 'islands' of fresh olivine. One sample (D140) is completely altered to serpentine and minor talc.

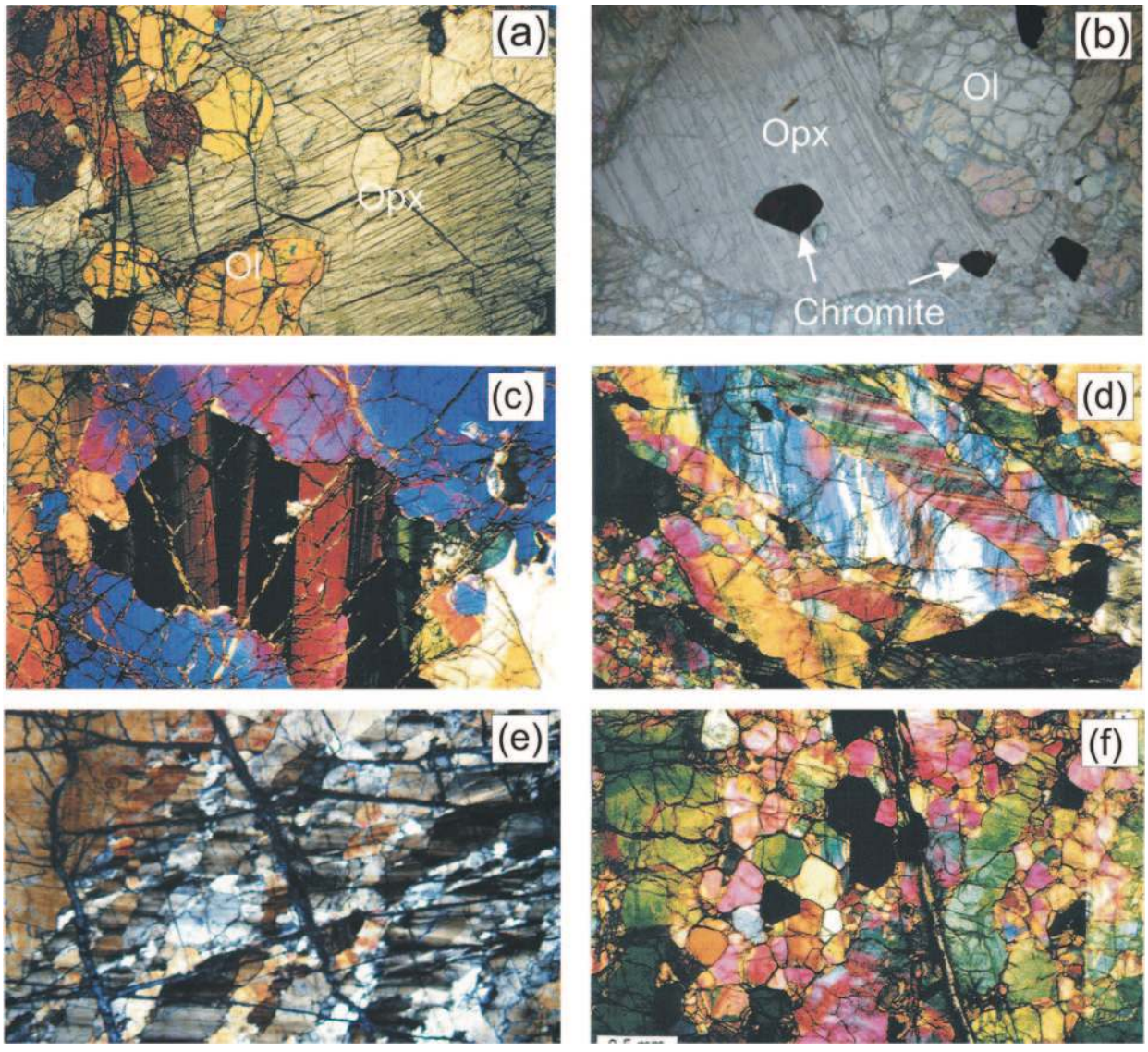

Fig. 3. Photomicrographs showing the textures of silicate rocks in the Luobusa ophiolite. (a) Harzburgite, opx surrounded by olivine; (b) transition zone dunite with opx and euhedral chromite; (c) and (d) kink-banding, mini kinking and boundaries of coarse olivine grains in dunites; (e) transition-zone dunite showing kink-banding in large olivine grains and olivine neoblasts; (f) high-temperature recrystallization of olivine neoblasts. All photos are 4 mm across.

Reaction zone

The dunite dykes in the cpx-bearing harzburgite generally range from 20 to 50 cm wide and most grade into the host peridotite over a few centimetres to a few tens of centimetres (Fig. 2a and b). Some of the dykes contain narrow bands of chromite (Fig. 2a), whereas others contain distinct bands of massive and disseminated chromitite (Fig. 2b). The chromitite bands consist of about 50–90 modal % magnesiochromite and have sharp contacts with the surrounding dunite (Fig. 2b). The dunites are similar in texture and mineralogy to those in the transition zone. In addition to olivine, they may contain trace amounts of diopside, orthopyroxene and chromite. The dunite grades smoothly into the host peridotite with increasing quantities of pyroxene (Fig 2a and b). The dunites are moderately altered to serpentine and talc, whereas the peridotites are very fresh.

SAMPLING METHODS AND ANALYTICAL TECHNIQUES

Representative samples were selected from the harzburgites, whereas the transition-zone dunites were sampled

Table 1: Detection limit, blank level and analytical results (ppb) of reference materials, PCC-1 (peridotite) and GeoPT-12 (serpentinite) (after Qi et al.*, 2004)*

	Detection limit (3σ)	Blank level	PCC-1						GeoPT-12	
			This work		Olive	Jain A		Eggins	This work $n = 6$	Potts
			$n = 6$	RSD%		A	B			
Y	0·0019	0·008	78·4 ± 1·9	2·4	–	–	–	87	403 ± 14	400
La	0·0084	0·23	50·1 ± 1·1	2·3	48	33	29	29	157 ± 9	150
Ce	0·0091	0·28	82·2 ± 3·7	4·6	71	60	56	53	291 ± 17	279
Pr	0·0025	0·045	8·83 ± 0·21	2·4	9·8	7·6	7·2	6·8	32·6 ± 1·5	30·8
Nd	0·0061	0·074	32·1 ± 2·9	9·2	32	26	28	25	134 ± 8	136
Sm	0·0011	0·013	5·96 ± 0·29	4·9	7·0	4·9	5·1	5	32·2 ± 1·3	37
Eu	0·0003	0·009	1·04 ± 0·06	5·8	2·0	0·9	1·00	1·1	6·38 ± 0·50	9·5
Gd	0·0010	0·010	5·29 ± 0·31	5·8	7·6	5·3	5·93	6·1	28·6 ± 1·2	42
Tb	0·0004	0·002	1·11 ± 0·09	8·4	1·6	1·0	1·12	1·2	6·92 ± 0·21	10
Dy	0·0021	0·027	9·57 ± 0·42	4·3	12	8·5	9·41	8·7	53·9 ± 2·6	57
Ho	0·0002	0·006	2·76 ± 0·22	7·9	3·1	2·3	2·69	2·7	12·7 ± 0·7	12
Er	0·0006	0·014	11·1 ± 0·8	7·2	12	10·0	11·3	11·3	39·2 ± 0·9	42
Tm	0·0001	0·003	2·43 ± 0·13	5·2	2·7	2·0	2·44	–	6·89 ± 0·31	7·5
Yb	0·0014	0·030	21·7 ± 1·1	5·1	23	20·0	22·1	21·3	49·5 ± 1·8	50
Lu	0·0004	0·006	4·42 ± 0·19	4·3	5·0	4·5	4·65	4·6	8·76 ± 0·50	9·2

Literature values: Olive (Olive *et al.*, 2001); Jain (Jain *et al.*, 2000): A indicates microconcentric nebulization and B indicates ultrasonic nebulization; Eggins (Eggins *et al.*, 1997); Potts (Potts *et al.*, 2003).

systematically along a single section (Fig. 1). To further investigate chemical and mineralogical differences between harzburgites and dunites, a typical dunite dyke with a band of chromitite was sampled systematically from the chromitite band to the host cpx-bearing harzburgite (Fig. 2b). Slices 2 cm thick and approximately 25 cm^3 in volume were taken sequentially across a transition of 20 cm (Fig. 2b). All samples were crushed and powdered to 200 mesh in an agate mill.

The compositions of silicate minerals and chromite were obtained using a JEOL JXA8800 microprobe at Dalhousie University, Canada, using an accelerating voltage of 15 kV and a beam current of 2 nA. A range of natural and synthetic standards and the manufacturer's ZAF correlation program were used for calibration. For major oxide concentrations, the precision was within 1–2% of the amount present, whereas the precision of trace elements analyses was between 2 and 10%.

Whole-rock major oxides and several trace elements were analysed with a Phillips PW2400 sequential X-ray fluorescence spectrometer at The University of Hong Kong. Fused glass discs were used for major oxides, whereas pressed powder pellets were used for trace-element determinations. The analytical precision was better than 5% for major elements and between 5 and 10% for trace elements.

Because ultramafic rocks have very low concentrations of REE, pre-concentration of these elements was carried out using $Fe(OH)_3$ and $Mg(OH)_2$ co-precipitation. Details of the sample preparation have been given by Qi *et al.* (2004). After separation of the major elements, the solutions were diluted approximately 60 times, compared with a dilution factor of 1000 in a normal acid digestion, and were then analysed for Y and REE using a VG Elemental Plasma-Quad Excell inductively coupled plasma-mass spectrometer (ICP-MS) at The University of Hong Kong. The precision of this method is typically better than 8% and the recovery of REE is more than 95% (Table 1) (Qi *et al.*, 2004).

Platinum group elements were pre-concentrated by fire assay using a combination of NiS fusion and Te co-precipitation (Zhou *et al.*, 2000; Sun *et al.*, 2001). After pre-concentration, the sample solutions were analysed by ICP-MS at The University of Hong Kong. Standard reference materials WPR-1 and TDB-1 were analysed periodically. Analytical precision was better than 10% for Ru, Rh and Ir, and 15% for Pd and Pt. Osmium data are not reported because it is difficult to control the loss of Os oxides during sample preparation (Sun *et al.*, 2001).

ANALYTICAL RESULTS

Mineral composition data are given in Table 2 and whole-rock major oxides and trace elements are listed in Tables 3 and 4. Most samples produced only a small loss on ignition (LOI), reflecting their weak serpentinization. A few dunite samples are extensively altered and have an LOI of >5%. One completely altered sample (D140, Table 4) has an LOI of 16·4%. In order to compare fresh and altered rocks, all bulk-rock analyses were normalized to 100% on an anhydrous basis. The normalized oxide values of the highly altered samples are very similar to those of the fresh samples, indicating little gain or loss of major oxides during alteration.

Mineral chemistry

Olivines in the harzburgites are compositionally uniform with Fo values of 90–92, slightly higher than those of olivines in most abyssal peridotites (average Fo = 90·8; Dick & Bullen, 1984). The dunites contain olivine with somewhat higher Fo values (91·5–93·5) than those in the harzburgite (Zhou, 1995), whereas olivine in the chromitites is highly magnesian (Fo = 95–98), indicating subsolidus Mg–Fe exchange with chromite (Roeder *et al.*, 1979). Orthopyroxenes in the harzburgites, dunites and chromitites are generally uniform in composition (En = 87·0–92·5), but their Al_2O_3 contents are variable and are in the range of ~1·5–4·0 wt % in harzburgites, 0·5–2·2 wt % in dunites and 0·5–1·25 wt % in chromitites (Fig. 4; Zhou, 1995).

The sparse clinopyroxenes are generally diopside with Al_2O_3 contents ranging from ~1·0 to 5·0 wt % for those in harzburgites, from 1·0 to 2·0 wt % for those in dunites and from 0·5 to 1·5 wt % for those in chromitites (Zhou, 1995). Clinopyroxenes in the dunites and chromitites have higher SiO_2 but lower Al_2O_3 and FeO than those in harzburgites (Table 2). Accessory chromites in the harzburgites have variable compositions with Cr-numbers [100Cr/(Cr + Al)] ranging from 22 to 65, which are lower than those of chromites in the dunites and chromitites.

The Al_2O_3 contents of both orthopyroxenes and clinopyroxenes in the harzburgites correlate negatively with the Cr-number of coexisting chromites, whereas Fo in olivine shows a positive correlation with the Cr-number (Fig. 4). Alumina contents in pyroxenes are known to be sensitive to the degree of mantle melting, decreasing systematically with increasing depletion of peridotites (e.g. Dick & Natland, 1996). The Al_2O_3 contents of orthopyroxenes in the Luobusa harzburgites (1·5–4·0 wt %) are generally lower than those in abyssal peridotites (2·19–5·0%) (Dick & Natland, 1996). Olivine compositions in the dunites vary significantly whereas the Cr-number of chromites remains relatively constant.

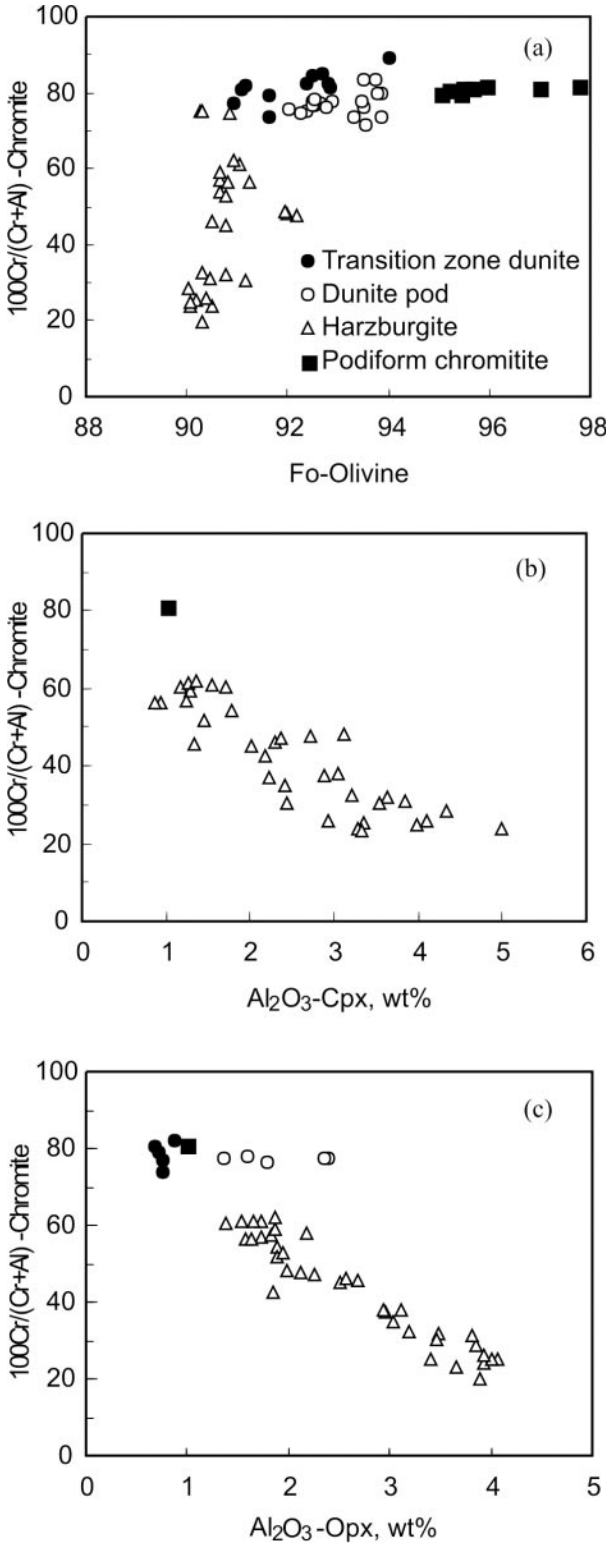

Fig. 4. Chemical compositions of minerals in the mantle sequence of the Luobusa ophiolite, southern Tibet. (a) Plots of Fo value of olivine versus Cr-number of chromite; (b) plots of Cr-number of chromite versus Al_2O_3 contents of clinopyroxene (cpx); (c) plots of Cr-number of chromite versus Al_2O_3 contents of orthopyroxene (opx).

Table 2: Representative compositions of olivine and pyroxenes from the mantle sequence of the Luobusa ophiolite, Southern Tibet

	Olivine																			
	Harzburgite					Dunite pods										Chromitite				
Sample:	L6	H14	H1	L17	L22	S4-3	ZHK10	L8	LH4	L16	L9	L13	ZHK8	S4	IIIV6	ZHK6-2	L26	L25	L27	S4
SiO_2	41·35	40·50	40·76	40·82	40·59	41·42	41·51	40·37	40·77	40·66	41·11	41·12	42·09	41·39	41·00	42·22	41·51	41·85	41·28	41·25
FeO	8·96	9·57	8·86	9·44	8·88	7·88	8·60	9·07	9·56	7·96	8·17	6·11	6·27	7·08	7·55	4·29	4·56	3·21	4·76	5·90
MnO	0·11	0·15	0·22	0·26	0·23	0·08	0·06	0·27	0·14	0·05	0·12	0·06	0·23	0·06	0·13	0·14	0·15	0·05	0·07	0·01
MgO	47·43	49·36	49·52	50·03	49·90	50·94	50·52	48·67	49·44	50·42	50·77	52·13	52·85	52·32	50·66	54·01	52·38	54·00	51·67	52·40
CaO	0·07	0·04	0·08	0·04	0·00	0·04	0·02	0·19	–	0·01	0·07	0·07	0·04	0·07	0·00	0·02	0·05	0·00	0·04	0·07
NiO	0·46	0·44	0·39	0·62	0·44	0·49	0·37	0·41	0·41	0·69	0·52	0·36	0·61	0·56	0·25	0·66	0·48	0·88	0·57	0·61
Total	98·47	100·02	99·76	101·17	100·03	100·74	101·05	99·20	100·18	101·05	100·57	99·72	102·16	101·35	99·21	101·44	98·93	99·94	98·27	100·44
Fo	90·31	90·05	90·67	90·18	90·71	91·94	91·23	90·28	90·08	91·82	91·61	93·78	93·54	92·89	92·16	95·60	95·19	96·73	95·02	94·04

	Clinopyroxene																			
	Cpx-harzburgite				Harzburgite						Dunite pods						Chromitite			
Sample:	L-w1	LH4-1	LH3-2	S4-4-h	ZHK11-1	L17-1	L22-2	L10-1	L19-1	L6-1	S4-a	S4-2-b	S4-2-c	IIIV6-14	IIIV6-15	IIIV6-18	IIIV6-1	IIIV6-11	IIIV6-13	ZHK-b
SiO_2	52·65	52·00	52·38	52·84	54·00	52·56	53·19	52·21	53·68	51·78	54·50	54·00	53·90	54·02	53·10	53·62	53·48	53·57	54·19	55·54
TiO_2	–	0·12	0·06	0·08	0·07	0·15	0·04	0·10	0·01	0·13	0·07	0·10	0·08	0·05	0·08	0·06	0·05	0·06	0·05	0·09
Al_2O_3	3·12	3·99	3·84	2·23	2·01	3·35	1·16	3·63	1·27	4·34	1·15	2·00	1·74	1·07	2·17	1·66	1·48	1·51	1·00	0·51
FeO	1·78	2·49	2·42	1·90	1·60	2·36	1·77	2·08	1·70	2·16	1·54	2·10	1·58	1·38	2·03	2·07	1·64	1·39	1·50	1·12
MgO	16·84	17·26	16·68	17·67	18·50	17·08	17·77	16·44	17·82	16·13	18·10	19·20	17·89	17·86	18·16	17·87	18·67	17·75	18·08	18·30
CaO	24·40	24·41	25·21	25·75	24·37	25·26	25·71	25·11	25·84	26·19	25·48	23·32	26·00	23·68	22·37	22·56	22·10	23·17	23·65	25·35
Cr_2O_3	0·80	1·05	1·13	0·75	0·88	0·66	0·86	1·23	0·61	1·23	0·63	0·93	0·54	0·78	1·15	0·97	0·90	1·06	0·84	0·45
Na_2O	0·10	0·21	0·33	0·27	0·14	0·26	0·22	0·41	0·15	0·09	0·33	0·19	0·27	0·17	0·16	0·21	0·18	0·19	0·13	0·33
Total	99·69	101·41	101·98	101·41	101·50	101·53	100·69	101·12	101·07	101·93	101·73	101·73	101·92	98·96	99·15	98·96	98·44	98·64	99·40	101·60
En	47·61	47·69	46·13	47·44	50·12	46·73	47·71	46·10	47·72	44·60	48·56	51·70	47·76	50·11	51·34	50·70	52·64	50·47	50·34	49·26

	Orthopyroxene																		
	Cpx-harzburgite					Harzburgite						Dunite pods				Chromitite			
Sample:	S4-4-g	LH4-2	LH4-3	LH4-4	LH3-1	H1-1	L12-3	H14-2	S4-3-c	L6A-1	L22-2	L19-1	L6-2	S4-a	S4-2-a	IIIV6-1	R67-a	IIIV6-3	IIIV6-4	IIIV6-16
SiO_2	55·76	55·51	55·03	55·17	55·59	56·24	56·02	54·73	56·47	56·65	57·73	56·43	55·58	56·74	56·34	56·80	58·72	57·72	57·64	57·49
Al_2O_3	2·95	3·40	3·71	3·62	3·20	1·74	1·79	3·67	2·68	1·95	0·52	1·74	3·85	1·60	2·39	1·58	0·80	0·77	0·89	0·82
FeO	4·81	6·45	6·18	6·16	5·95	5·82	5·72	6·26	4·94	5·91	5·13	5·56	6·39	4·68	4·90	5·03	2·76	4·03	3·90	4·21
MgO	33·19	33·50	33·15	33·22	33·67	34·17	33·92	32·99	35·22	34·41	35·65	34·09	33·57	35·30	34·60	34·73	37·07	36·89	36·53	36·81
CaO	2·60	0·86	0·85	0·48	0·99	0·64	1·16	0·71	0·74	1·24	0·25	0·74	0·48	0·81	0·99	0·96	0·52	0·31	0·24	0·28
Cr_2O_3	0·65	0·34	0·65	0·65	0·60	0·42	0·57	0·68	0·75	0·73	0·14	0·58	0·81	0·61	0·65	0·63	0·58	0·82	0·48	0·44
Na_2O	0·15	0·15	0·23	0·09	0·17	0·14	0·10	0·06	0·12	0·15	0·19	0·09	0·19	0·15	0·10	0·02	0·09	0·00	0·00	0·00
Total	100·21	100·07	99·80	99·31	100·00	99·02	99·17	99·36	101·09	101·22	99·46	99·14	101·25	99·74	99·87	100·01	100·54	100·56	99·99	100·04
En	87·91	88·77	89·05	89·73	89·26	90·18	89·36	89·14	91·44	89·11	92·10	90·32	89·51	91·67	90·90	90·82	95·07	93·70	93·94	93·50

Bulk-rock compositions

Chemical variations across the dunite dyke

Variations in mineral chemistry across the transitional boundary between a dunite dyke and cpx-bearing harzburgite were reported by Zhou *et al.* (1996). Surprisingly, the chemical compositions of chromite, olivine, orthopyroxene and clinopyroxene through the reaction zone span the complete range of these minerals in the entire mantle sequence of the Luobusa ophiolite. For example, the Cr-number of chromite varies regularly from 20 in the cpx-bearing harzburgite to 80 in the chromitite band.

Regular mineralogical and chemical variations are observed across the dyke boundary (Fig. 5), with a gradual transition from the host cpx-bearing harzburgite to harzburgite to dunite reflecting a systematic decrease in the amount of pyroxene (Fig. 2b). This transition is marked by systematic decreases in SiO_2, CaO, Al_2O_3, Zn, Sc, Y, V, Ga and Cu and increases in MgO, Mg-number and Ni (Fig. 5a and b). Iron remains nearly constant across the transition. These changes result in a significant increase in Mg/Si and Ni/Cu ratios and a decrease in CaO/Al_2O_3 ratios from the cpx-bearing harzburgite to the dunite. The dunite is relatively uniform in bulk-rock composition, but shows a steady increase in Mg-number and a very small increase in SiO_2 toward the chromitite band in the centre. One sample (R6, Table 3) is transitional from harzburgite to dunite. The sharp boundary between the dunite and chromitite is marked by abrupt increases in Zn, Ni, V and Ga, but Sc and Cu show no change across this boundary, leading to a slight increase in the Ni/Cu ratio (Table 3 and Fig. 5b).

The HREE, for example Lu, show interesting patterns, decreasing from the cpx-bearing harzburgite to the dunite, and again to the chromitite (Fig. 5c). La and other LREE show relatively small variations, increasing slightly from cpx-bearing harzburgite to dunite (Fig. 5c). The chromitite band has much higher Ir, Ru and Rh but slightly lower Pd than both the dunite and harzburgite. Ir, Ru and Rh show only small variations from the cpx-bearing harzburgite to the dunite whereas Pt and Pd, and thus the Pd/Ir ratio, decrease across this zone. Pt/Pd ratios of the dunite and harzburgite are relatively constant and lower than those of the chromitites. In general, Pd and HREE display similar variations across these lithological and mineralogical transitions.

Chemical variations throughout the whole mantle sequence

The harzburgites and cpx-bearing harzburgites are very uniform in composition, ranging from 43·8 to 44·8 wt % SiO_2 and 43·6 to 45·0 wt % MgO, although the cpx-bearing varieties have somewhat higher Al_2O_3 (Tables 3 and 4).

Table 3: Major oxide, trace element, REE and PGE analyses of rocks from the reaction zone around the chromitite band, Luobusa ophiolite, southern Tibet

	Chromitite		Dunite				Harzburgite			
Sample:	R1	R2	R3	R4	R5	R6	R7	R8	R9	R10
Major oxides (wt %)										
SiO_2	–	–	42·19	41·67	41·70	41·81	43·93	44·45	44·32	43·65
TiO_2	–	–	0·01	0·01	0·01	0·01	0·01	0·01	0·01	0·01
Al_2O_3	–	–	0·35	0·35	0·41	0·57	1·07	1·23	1·37	1·25
Fe_2O_3	–	–	6·86	7·11	7·35	7·40	7·19	7·13	7·31	7·36
MnO	–	–	0·09	0·10	0·11	0·10	0·11	0·11	0·11	0·10
MgO	–	–	49·92	49·99	49·64	49·00	45·59	44·60	43·66	44·33
CaO	–	–	0·09	0·10	0·19	0·56	1·55	2·02	2·20	1·79
Na_2O	–	–	0·01	0·01	0·01	0·01	0·01	0·01	0·01	0·01
Cr_2O_3	–	–	0·46	0·65	0·58	0·53	0·54	0·44	1·00	1·49
S	–	–	0·38	0·40	0·32	0·33	0·41	0·41	0·44	0·38
LOI	–	–	5·75	5·16	5·23	4·72	2·09	2·07	2·13	3·72
Trace elements (ppm)										
Zn	165	209	5	7	11	13	17	20	19	20
Co	–	–	130	135	144	141	137	136	134	140
V	236	276	14	14	17	24	44	50	64	65
Ni	4844	4368	2981	2945	2914	2756	2285	2195	2163	2294
Cu	5·70	6·40	6·36	5·99	5·31	6·47	12·27	35	33	22
Sc	5·90	6·20	6·14	6·02	6·14	8·45	15·00	16·00	17·70	15·40
Zr	14·58	17·33	20·69	20·99	20·97	20·51	22·30	20·68	21·71	19·53
Nb	8·16	7·86	16·36	17·75	18·25	17·02	17·21	17·02	17·58	14·98
Ba	11·03	24·97	22·67	20·47	15·09	19·87	19·10	28·21	19·75	13·45
Ga	10·18	11·88	1·10	1·05	1·09	1·23	1·64	1·77	1·94	1·99
Y and REE (ppb)										
Y	480	300	72	80	88	133	564	907	881	712
La	25·78	10·26	11·08	6·85	4·74	4·63	5·65	8·72	7·41	5·29
Ce	61·00	21·89	21·12	11·87	7·78	7·87	9·44	7·64	12·71	8·46
Pr	7·55	2·77	1·96	1·33	1·06	1·02	1·44	2·46	1·78	1·29
Nd	24·83	12·70	5·62	5·22	4·44	4·08	8·76	14·65	11·77	7·30
Sm	8·45	5·09	2·48	2·26	2·21	2·96	7·65	13·97	13·68	9·38
Eu	3·38	1·98	2·25	2·06	2·83	3·40	7·68	8·13	8·82	8·00
Gd	11·04	7·27	3·59	3·41	3·78	5·63	20	32	34	24
Tb	2·46	1·81	0·89	0·90	0·94	1·58	6·02	9·49	9·70	6·93
Dy	16·13	13·76	7·18	7·68	9·00	14	56	88	88	65
Ho	3·80	3·50	2·09	2·22	2·58	4·00	15·1	23	22	18
Er	13·0	12·0	9·4	10·2	10·5	14·3	52·4	80	76	64
Tm	2·20	2·05	2·07	2·20	2·13	2·69	9·09	14	12	11
Yb	17	14	19	20	19	24	67	98	83	83
Lu	3·35	2·70	4·12	3·90	4·21	4·54	11·53	15·68	13·27	13·74
PGE (ppb)										
Ir	64	74	3·93	6·13	5·56	3·98	3·72	3·05	3·23	4·50
Ru	48	55	3·55	5·94	6·37	5·79	7·61	7·27	5·31	5·27
Rh	4·10	4·55	0·54	0·97	0·72	1·02	1·53	1·36	0·99	1·13
Pt	4·75	6·05	1·13	3·50	1·70	5·28	7·68	8·74	4·86	4·44

	Chromitite		Dunite				Harzburgite			
Sample:	R1	R2	R3	R4	R5	R6	R7	R8	R9	R10
Pd	1·21	1·60	1·59	2·35	1·71	4·45	7·95	7·63	5·48	4·78
Mg/Si	–	–	1·75	1·77	1·76	1·73	1·53	1·48	1·45	1·50
Mg-number	–	–	94	93	93	93	93	93	92	92
CaO/Al_2O_3	–	–	0·26	0·27	0·47	1·00	1·44	1·64	1·61	1·44
Ni/Cu	850	683	469	492	549	426	186	62	65	105
La/Sm	3·05	2·01	4·46	3·04	2·15	1·56	0·74	0·62	0·54	0·56
Tb/Lu	0·73	0·67	0·22	0·23	0·22	0·35	0·52	0·61	0·73	0·50
La/Lu	7·70	3·80	2·69	1·76	1·13	1·02	0·49	0·56	0·56	0·39
Pd/Ir	0·02	0·02	0·40	0·38	0·31	1·12	2·14	2·50	1·70	1·06
Pt/Pd	3·91	3·78	0·71	1·49	1·00	1·19	0·97	1·15	0·89	0·93

LOI, loss on ignition; –, data are not available.

Normalized compositions of the transition-zone dunite are relatively uniform despite large differences in the degree of alteration as indicated by the LOI. SiO_2 in the dunites ranges from 38·1 to 42·5 wt %, whereas MgO varies from 46·1 to 51·6 wt % (Table 4). Total iron ranges from 5·92 to 10·1 wt % and correlates inversely with MgO. Dunite dykes and pods all fall within the compositional ranges defined by the transition-zone dunites and are somewhat more uniform. As expected, all of the dunites have lower average SiO_2, Al_2O_3, CaO, TiO_2 and V contents and higher average MgO contents than the harzburgites.

All of the peridotites and dunites in the Luobusa mantle sequence have variable and low REE concentrations, with HREE ranging from 0·1 to 0·8 × chondrite, MREE from 0·05 to 0·2 × chondrite and LREE from 0·01 to 1·0 × chondrite (Table 4). Although their total REE contents vary, samples of each lithology have relatively consistent chondrite-normalized REE patterns (Fig. 6). Cpx-bearing harzburgite, including reaction zone samples R7, R8, R9 and R10, have 'spoon-shaped' chondrite-normalized REE patterns (Fig. 6a and e) nearly identical to those described for cpx-rich harzburgites from the Oman ophiolite (see Godard *et al.*, 2000). Only two samples of harzburgite are available from Luobusa and both of these have concave-upward, U-shaped REE patterns (Fig. 6b). One sample (L-22) has a small positive Eu anomaly. These harzburgite patterns are similar to those of the Maqsad diapir harzburgites of the Oman ophiolite, several of which also show weak positive Eu anomalies (Godard *et al.*, 2000). All of the Luobusa dunites, including those from pods (Fig. 6c), the transition zone (Fig. 6d) and the investigated reaction zone (Fig. 6e) have well-developed concave-upward, U-shaped REE patterns enriched in both LREE and HREE, but depleted in MREE. Enrichment in LREE is variable, with $La/Sm_{(n)}$ ratios generally between 2 and 15. All of the dunite samples from the reaction zone have small positive Eu anomalies (Fig. 6e), as do some from the transition zone (Fig. 6d). Even though the transition-zone dunites have chondrite-normalized REE patterns similar to those of the reaction-zone dunite, they have significantly lower total REE abundances. The trace-element contents of the Luobusa peridotites are thus distinctly different from those of typical MORB peridotites, which are LREE depleted and have much higher HREE contents. These patterns are similar to those reported for mantle peridotites in Oman (Godard *et al.*, 2000; Takazawa *et al.*, 2003).

Copper and Ni correlate negatively in both chromitites and harzburgites, whereas dunites are generally low in Cu and have variable Ni contents (Fig. 7). Chromitites have higher Ni contents than the harzburgites at a given Cu content, resulting in two different but nearly parallel trends in Fig. 7. The reaction-zone samples show a systematic variation in Cu–Ni contents from the host cpx-bearing harzburgite (Samples R8, R9; Fig. 7) to the reaction-zone dunite (Samples R3–6, Fig. 7). As expected, all of the dunites have higher Ni/Cu ratios than the harzburgites.

In a plot of Pd versus Pt, all samples have chondrite ratios (Fig. 8a). Iridium contents generally increase from harzburgite to dunite to chromite, whereas Pd remains relatively constant (Fig. 8b). The harzburgites have slightly higher Pd/Ir ratios than the dunites, whereas the chromitites have much lower ratios than the peridotites (Fig. 9; Table 4). In a plot of Pd/Ir versus Ni/Cu, there is generally a negative correlation between Pd/Ir and Ni/Cu in the peridotites, but little variation of Pd/Ir over a wide range of Ni/Cu in the chromitites (Fig. 9).

Table 4: Major oxide, trace element, REE and PGE analyses of rocks from the Luobusa ophiolite, southern Tibet

	Transition-zone dunite												
Sample:	Do	D5	D10	D15	D20	D25	D30	D55	D65	D70	D75	D80	D85
Major oxides (wt %)													
SiO_2	41·36	38·07	42·45	40·94	41·73	42·22	40·33	42·04	40·76	40·35	40·68	42·00	42·52
TiO_2	0·01	0·01	0·01	0·01	0·01	0·01	0·01	0·01	0·01	0·01	0·01	0·01	0·01
Al_2O_3	0·27	0·25	0·31	0·23	0·21	0·20	0·21	0·23	0·22	0·21	0·19	0·25	0·25
Fe_2O_3	8·05	9·14	8·99	9·58	7·32	7·03	8·46	8·29	7·88	10·75	8·38	8·69	10·08
MnO	0·12	0·12	0·14	0·13	0·11	0·11	0·12	0·11	0·10	0·12	0·11	0·13	0·13
MgO	49·45	51·56	46·88	48·41	49·82	49·72	50·00	48·68	50·42	47·93	49·98	47·99	46·12
CaO	0·29	0·46	0·77	0·23	0·30	0·27	0·25	0·25	0·09	0·08	0·14	0·51	0·49
Na_2O	0·06	0·06	0·09	0·07	0·06	0·07	0·05	0·07	0·06	0·06	0·06	0·07	0·11
Cr_2O_3	0·39	0·32	0·35	0·41	0·45	0·38	0·57	0·33	0·46	0·49	0·45	0·34	0·29
LOI	4·64	2·91	4·03	4·54	6·93	5·86	4·95	13·84	3·21	4·90	5·49	8·37	10·41
Trace elements (ppm)													
Zn	40	38	44	45	35	35	42	31	41	48	36	44	35
Co	653	716	66	79	71	65	76	64	70	75	72	58	64
V	17	16	27	20	13	13	22	12	16	23	13	27	15
Ni	2476	2568	2113	2375	2433	2522	2431	2180	2539	2476	2573	2052	2131
Cu	8·99	7·38	8·70	7·47	6·98	7·36	5·24	9·81	6·53	7·30	7·50	7·59	5·24
Y and REE (ppb)													
Y	20	20	28	11	20	23	11	13	19	7	19	30	10
La	9·88	5·70	7·94	6·49	9·91	9·76	2·13	1·89	2·61	2·21	3·62	7·82	2·16
Ce	17·99	10·41	14·50	17·84	15·82	15·59	3·17	2·90	3·84	3·57	5·44	13·30	3·26
Pr	2·13	1·18	1·28	1·33	2·10	1·76	0·41	0·33	0·46	0·44	0·58	1·35	0·39
Nd	8·10	4·79	3·38	2·46	5·87	4·64	1·28	1·16	1·41	1·26	1·75	4·12	1·37
Sm	1·60	0·85	0·94	0·27	1·28	1·23	0·26	0·23	0·20	0·20	0·34	0·69	0·19
Eu	0·41	0·28	0·20	0·20	0·21	0·18	0·15	0·15	0·17	0·13	0·24	0·35	0·15
Gd	1·39	1·10	1·54	0·61	1·93	1·44	0·38	0·42	0·51	0·28	0·42	1·30	0·40
Tb	0·27	0·23	0·44	0·11	0·38	0·29	0·08	0·11	0·13	0·06	0·14	0·31	0·09
Dy	2·07	2·09	3·46	1·00	2·97	2·49	0·88	0·91	1·48	0·42	1·55	3·08	0·75
Ho	0·68	0·72	1·25	0·33	0·95	0·75	0·32	0·44	0·63	0·22	0·57	1·00	0·31
Er	2·86	2·99	4·76	1·76	3·58	3·32	1·64	1·87	3·25	1·09	3·13	4·24	1·75
Tm	0·72	0·70	1·00	0·43	0·78	0·78	0·41	0·53	0·80	0·38	0·70	0·98	0·46
Yb	6·58	6·55	9·21	4·49	7·30	6·66	4·40	5·41	7·60	4·83	7·33	8·62	5·46
Lu	1·41	1·43	1·84	1·09	1·47	1·49	1·03	1·14	1·73	1·34	1·67	1·91	1·44
PGE (ppb)													
Ir	5·72	6·16	5·13	6·32	5·11	5·33	4·54	5·24	4·17	5·01	5·77	4·63	6·01
Ru	10·80	7·72	8·41	10·70	7·12	10·32	10·04	9·80	7·41	8·26	8·92	8·62	8·92
Rh	0·75	0·64	1·57	1·06	0·52	0·42	0·73	1·09	0·52	0·79	0·59	1·42	1·35
Pt	2·02	1·61	9·67	3·17	1·18	1·61	1·84	3·99	2·10	1·91	1·95	9·02	8·78
Pd	3·23	3·57	4·93	3·04	1·68	1·99	2·97	3·06	2·40	1·92	1·73	5·13	4·19
Mg/Si	1·76	2·00	1·63	1·74	1·76	1·74	1·83	1·71	1·82	1·75	1·81	1·69	1·60
Mg-number	92	92	91	91	93	93	92	92	93	90	92	92	90
CaO/Al_2O_3	1·08	1·83	2·47	1·00	1·47	1·32	1·20	1·05	0·40	0·40	0·72	2·04	2·00
Ni/Cu	275	348	243	318	349	343	464	222	389	339	343	271	407
La/Sm-n	3·87	4·19	5·28	15·16	4·84	4·97	5·16	5·21	8·11	6·95	6·60	7·13	7·15
Tb/Lu	0·13	0·11	0·16	0·07	0·17	0·13	0·05	0·06	0·05	0·03	0·06	0·11	0·04
La/Lu	0·71	0·41	0·44	0·61	0·69	0·67	0·21	0·17	0·15	0·17	0·22	0·42	0·15
Pd/Ir	0·56	0·58	0·96	0·48	0·33	0·37	0·65	0·58	0·58	0·38	0·30	1·11	0·70
Pt/Pd	0·63	0·45	1·96	1·04	0·71	0·81	0·62	1·30	0·88	1·00	1·13	1·76	2·09

	Transition-zone dunite			Dunite pods		Cpx-harzburgite			Harzburgite	
Sample:	D140	D145	D150	L16	L18	L6	L17	LH5	L22	L12
Major oxides (wt %)										
SiO_2	41·65	40·36	40·85	40·91	40·49	43·82	44·83	–	44·40	44·72
TiO_2	0·01	0·01	0·01	0·02	0·02	0·03	0·04	–	0·02	0·02
Al_2O_3	0·26	0·22	–	0·08	0·51	1·17	1·76	–	0·74	0·66
Fe_2O_3	5·92	7·47	6·61	8·64	6·80	9·07	8·60	–	8·56	8·41
MnO	0·11	0·10	0·10	0·14	0·11	0·15	0·15	–	0·15	0·13
MgO	51·12	51·13	51·56	49·61	51·50	43·56	42·20	–	45·00	44·99
CaO	0·29	0·20	0·16	0·14	0·05	1·77	1·91	–	0·65	0·69
Na_2O	0·07	0·07	0·07	–	–	–	–	–	–	–
Cr_2O_3	0·57	0·46	0·36	0·46	0·50	0·43	0·49	–	0·47	0·36
LOI	16·40	12·88	12·85	7·10	2·40	2·00	4·70	–	2·90	2·60
Trace elements (ppm)										
Zn	37	42	33	41	27	54	42	–	45	46
Co	63	61	61	–	–	–	–	–	–	–
V	14	16	15	15	8	60	66	–	34	37
Ni	2175	2237	2098	2560	–	2261	2045	–	2257	2308
Cu	5·22	5·71	7·97	5·00	–	24	28	–	13	16
Y and REE (ppb)										
Y	15	23	18	9	633	702	909	653	898	1091
La	6·34	15·47	2·17	4·85	21·41	8·88	5·70	3·69	244·23	91·55
Ce	9·48	30·01	3·45	7·76	36·39	8·63	9·16	5·39	497·86	157·88
Pr	1·15	2·63	0·47	0·86	4·30	1·44	1·24	0·73	55·99	17·98
Nd	4·00	8·20	1·75	2·80	14·74	5·93	7·83	6·07	208·12	62·45
Sm	1·18	2·69	0·46	0·99	3·05	5·20	12·55	10·40	39·55	13·29
Eu	0·18	0·30	0·16	0·21	1·21	3·18	6·12	4·97	8·53	3·57
Gd	0·94	1·56	0·52	0·66	3·98	19·76	34·16	24·88	43·05	17·43
Tb	0·18	0·24	0·18	0·08	0·80	6·23	9·97	7·01	7·11	3·84
Dy	1·80	2·38	1·59	0·62	5·57	64·03	91·69	63·45	45·72	29·72
Ho	0·57	0·68	0·55	0·25	1·52	17·46	22·86	16·56	11·05	8·13
Er	2·51	3·05	2·68	0·95	6·18	63·74	77·97	56·13	35·44	29·39
Tm	0·57	0·66	0·64	0·22	1·24	11·44	13·11	9·07	6·11	5·57
Yb	5·62	6·00	5·93	2·74	11·01	90·06	94·74	67·47	43·35	42·95
Lu	1·22	1·32	1·40	0·73	2·29	15·14	15·62	11·45	7·98	7·85
PGE (ppb)										
Ir	5·74	5·44	4·14	6·53	5·75	5·52	4·27	–	5·56	1·72
Ru	11·37	12·62	7·43	–	–	–	–	–	–	–
Rh	0·58	0·66	0·52	1·51	0·68	1·59	1·28	–	2·05	0·65
Pt	1·44	2·47	2·06	6·55	1·60	8·18	7·16	–	8·44	2·13
Pd	2·81	2·00	3·03	3·34	0·90	7·60	7·87	–	4·86	3·61
Mg/Si	1·81	1·87	1·86	1·79	1·88	1·47	1·39	–	1·49	1·48
Mg-number	94	93	94	92	94	90	91	–	91	91
CaO/Al_2O_3	1·09	0·89	0·54	1·75	0·10	1·51	1·09	–	0·88	1·05
Ni/Cu	416	392	263	512	–	94	73	–	174	144
La/Sm-n	3·37	3·60	2·96	3·06	4·40	1·07	0·28	0·22	3·86	4·31
Tb/Lu	0·10	0·12	0·09	0·07	0·23	0·27	0·43	0·41	0·59	0·33
La/Lu	0·53	1·19	0·16	0·68	0·96	0·06	0·04	0·03	3·13	1·19
Pd/Ir	0·49	0·37	0·73	0·51	0·16	1·38	1·84	–	0·87	2·10
Pt/Pd	0·51	1·23	0·68	1·96	1·78	1·08	0·91	–	1·74	0·59

LOI, loss on ignition; –, data are not available. Major oxides and PGEs for samples L16, L18, L6, L17, LH5 and L22 were also reported by Zhou (1996).

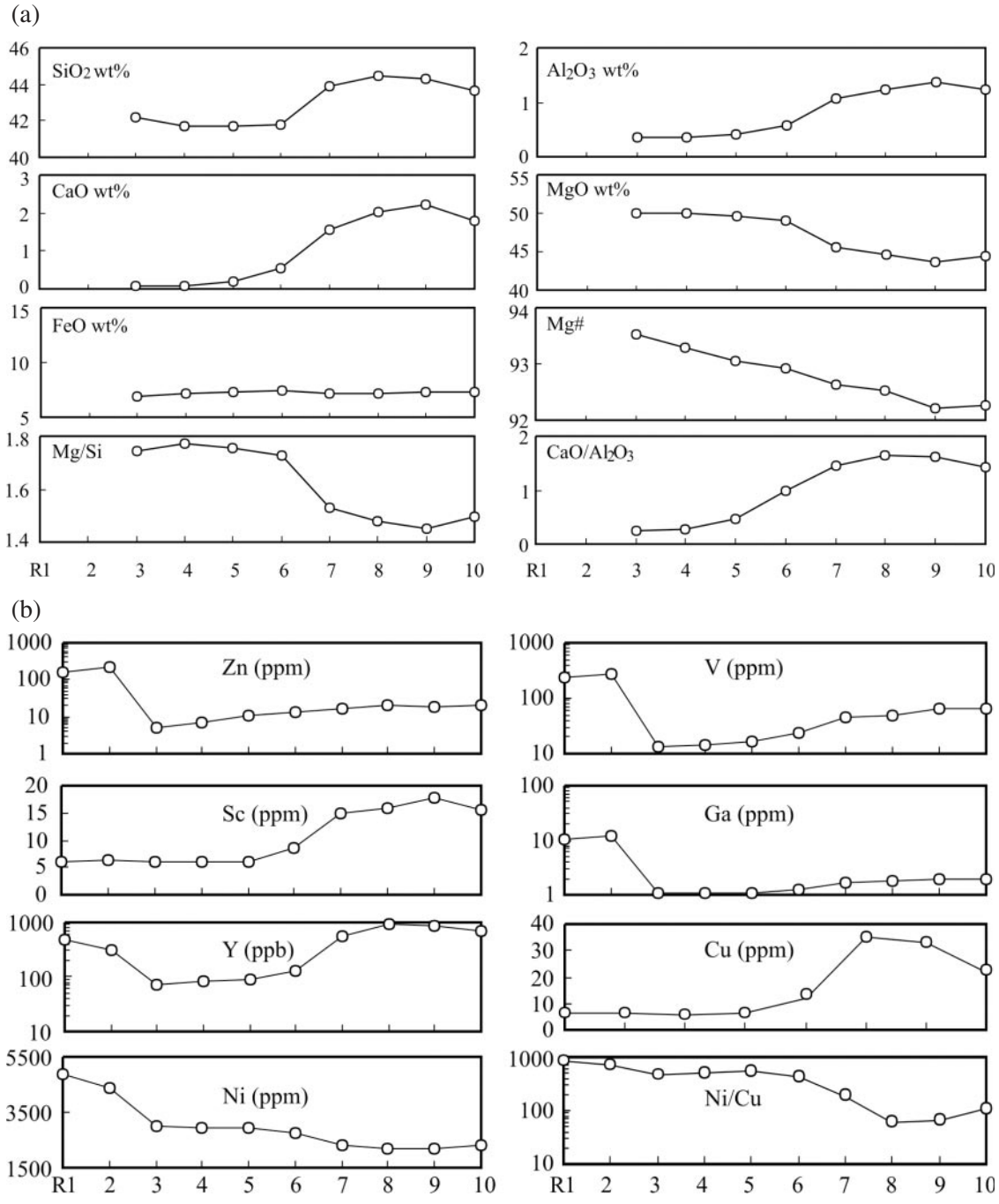

Fig. 5. Chemical variations in the reaction zone from cpx-bearing harzburgite to harzburgite to dunite to chromitite. (a) Major oxides (wt %) SiO_2, Al_2O_3, CaO, MgO and FeOt, Mg-number, and Mg/Si and CaO/Al_2O_3 ratios; (b) trace elements (ppm) Zn, V, Sc, Ga, Y, Cu and Ni, and Ni/Cu ratio; (c) trace elements (ppb), PGE (Ir, Ru, Rh, Pt and Pd) and ratios (Pd/Ir and Pt/Pd), and REE (La, Eu, Tb and Lu) and ratios (La/Sm, Tb/Lu and La/Lu). The location of samples R1–R10 is indicated in Fig. 2b.

Mantle-normalized siderophile element (Ni, PGE and Cu) plots are shown in Fig. 10. The harzburgites and cpx-bearing harzburgites have nearly identical patterns showing very slight enrichment in Pd and depletion in Cu (Fig. 10a and b). Dunites from pods and envelopes have generally inclined patterns with very slight enrichment in Ni and depletion in Pt, Pd and Cu (Fig. 10c). In the transition-zone dunites, two types of PGE patterns are recognized: relatively flat patterns enriched in PPGE (Pd subgroup; PGE), similar to those of the harzburgites, and patterns with negative Pt, Pd and Cu anomalies (Fig. 10d). These patterns are very similar to those of the dunite pods

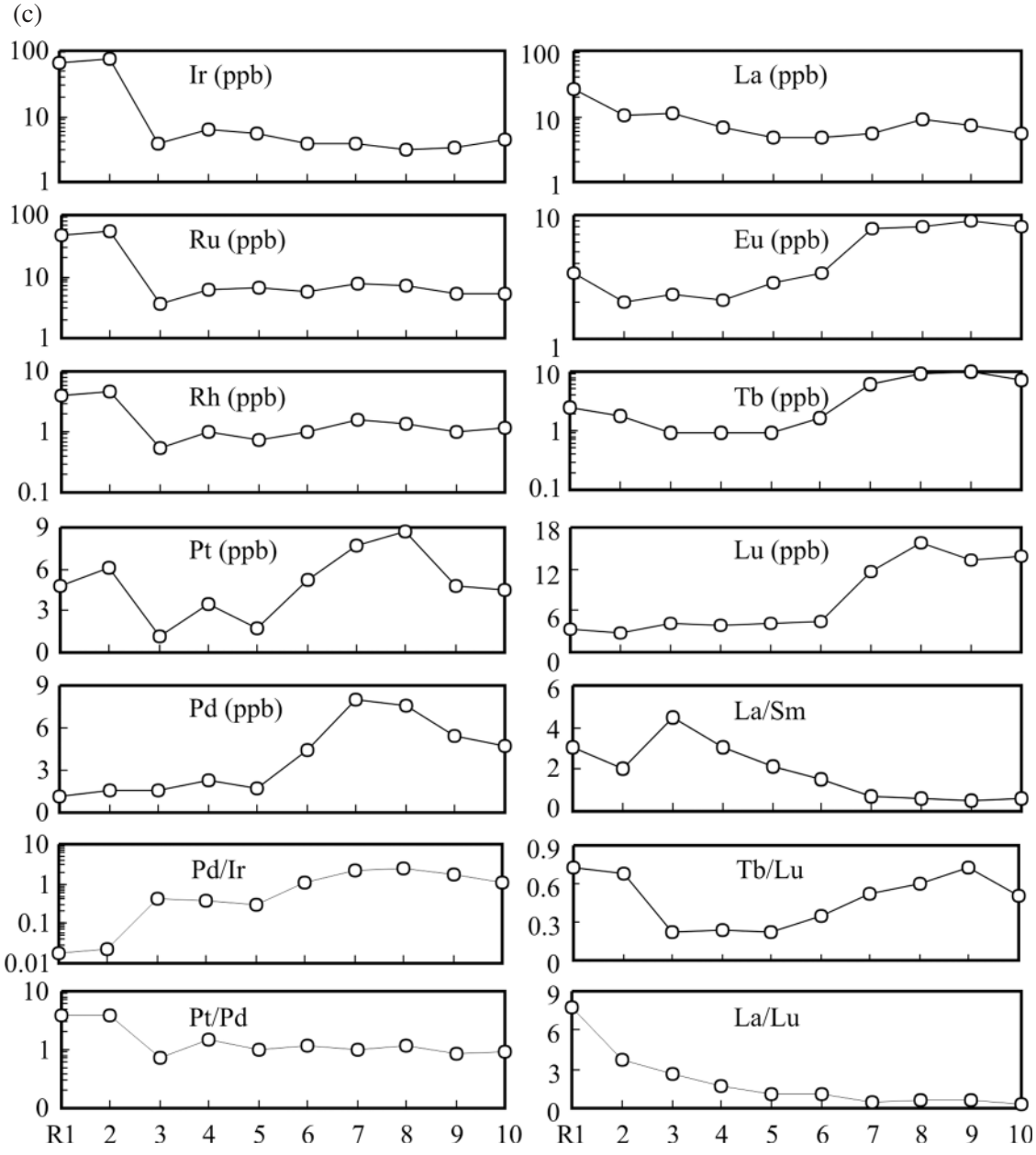

Fig. 5. *Continued*

(Fig. 10c) and reaction-zone dunites (samples R3 and R4, Fig. 10e). Two of the transition-zone dunites have patterns almost identical to those of the harzburgite. Samples from the reaction zone have variable patterns (Fig. 10e); samples R7, R8, R9 and R10 have patterns similar to those of the other harzburgites and cpx-bearing harzburgites, samples R3 and R4 have patterns identical to those of the dunite pods and envelopes, and samples R5 and R6 have patterns transitional between the harzburgites and dunites. Samples R1 and R2 (chromitites) are enriched in Ir, Ru and Rh (Ir subgroup; IPGE) and depleted in Pt, Pd (Pd subgroup; PPGE) and Cu, as are samples from podiform chromitites (Fig. 10f).

DISCUSSION

REE and PGE data contain essential information about the formation of mantle rocks, but few studies present data for both groups of elements because of the difficulty of obtaining high-quality REE data. The REE data presented in this paper were obtained by a new technique which greatly improves the recovery of REE and the

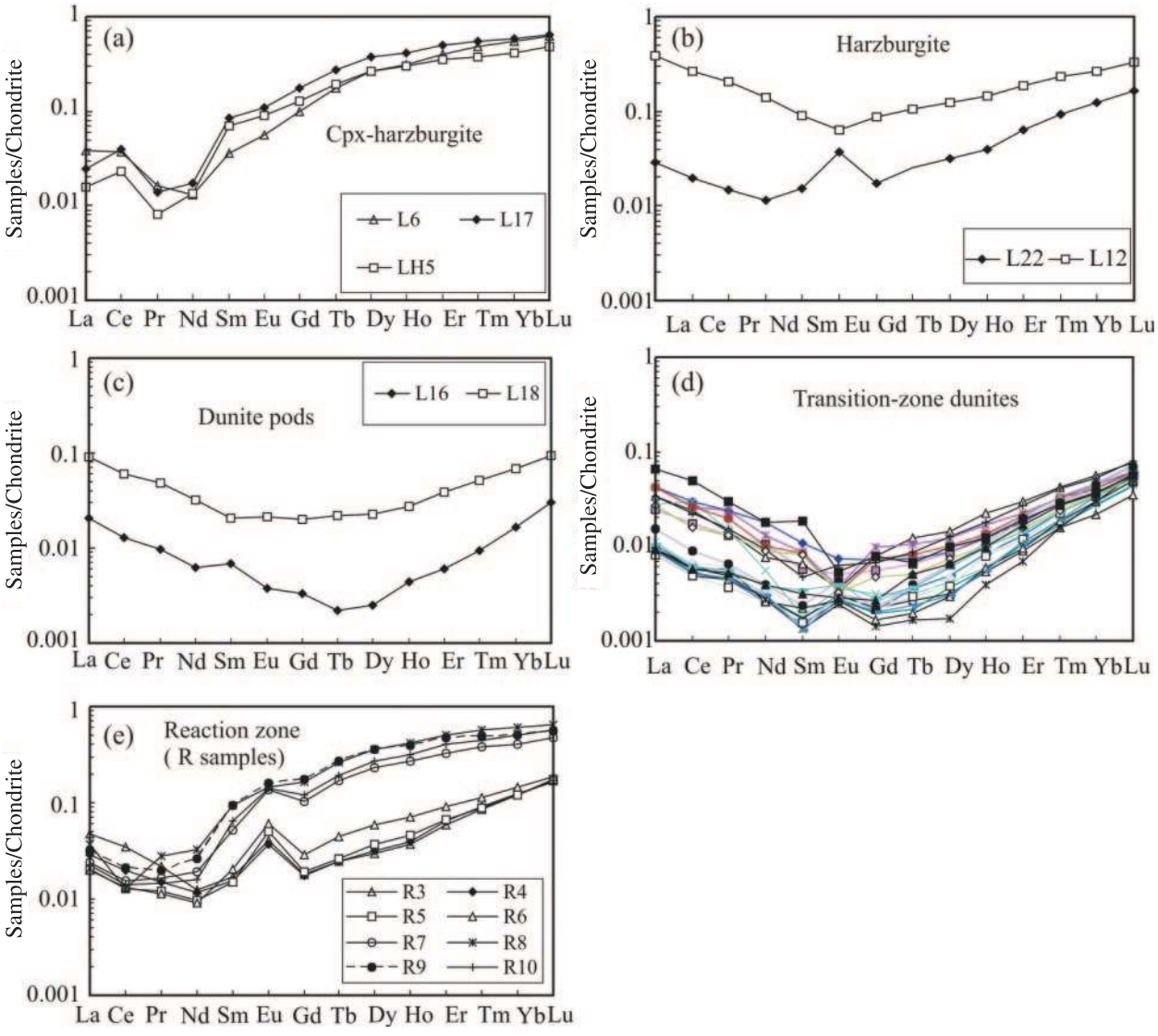

Fig. 6. Chondrite-normalized REE patterns of mantle rocks from the Luobusa ophiolite. (a) Three cpx-harzburgite samples; (b) two harzburgite samples; (c) two samples of dunite pods; (d) all samples from the transition zone; (e) eight samples from the reaction zone.

precision of the analyses (Qi *et al.*, 2004). In order to better understand the processes involved in the formation of Luobusa mantle rocks, we have collected data for all of the different lithologies and have undertaken a detailed study of a melt–rock reaction zone surrounding a dunite dyke. By examining the chemical and mineralogical changes produced by melt–rock reaction on a small scale, we can better constrain the processes that affected the entire mantle section. Thus, we first discuss the chemical changes recorded in a known melt–rock reaction zone, then examine the implications of these data for the formation of other mantle rocks in the Luobusa ophiolite, and finally consider the broader application of our findings.

Effects of alteration on the Luobusa mantle rocks

REE and PGE are generally considered to be relatively immobile during low-temperature alteration. However, some elements, such as Eu, can be modified somewhat by hydrothermal processes. Most of the peridotites and dunites examined in this study are unusually fresh, as indicated by their petrography and low LOI. However, some of the dunites show moderate to high degrees of serpentizition and one sample (D140, Table 4) is completely altered. The LOI of these samples correlates well with the degree of alteration determined petrographically. Normalization of the major oxides on a dry-weight

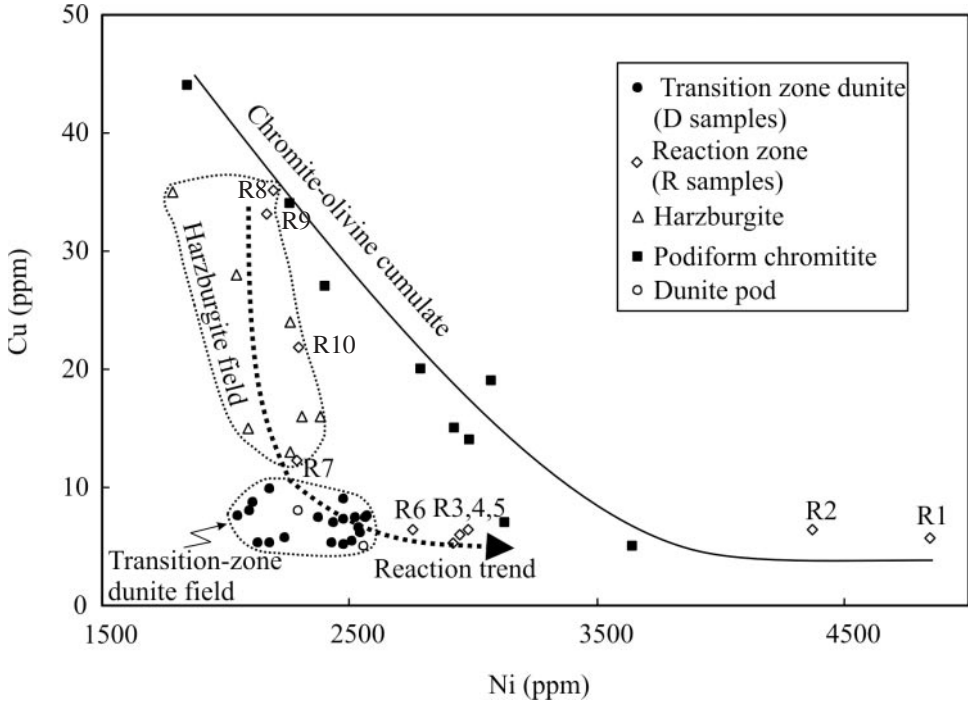

Fig. 7. Plot of Cu versus Ni content of the chromitites and dunites in the transition zone of the Luobusa ophiolite. Reaction zone samples (R1–10) have the same numbers as samples in Figs 2 and 5. Best-fit lines are hand-drawn.

basis indicates that the alteration mainly involved hydration with little gain or loss of major oxides. Because some of the samples show small, but distinct, positive Eu anomalies, we also investigated the effect of alteration on the REE. However, the REE do not show any correlation with LOI and the observed degree of alteration. Thus, we believe that the small Eu anomalies are because of other processes, as discussed below.

Origin of the chromitite–dunite dykes and their relationship to the harzburgites

Dunite veins and dykes are common in the mantle sections of ophiolites, particularly immediately beneath the transition-zone dunites. The concentration of dykes and veins at this level and their proximity to the massive dunites above suggest that they may be produced by similar processes. An understanding of the physical and chemical relationships between the dykes and the host peridotites is essential for placing constraints on their mode of origin.

Both the physical and chemical changes observed across the harzburgite–dunite dyke contacts could theoretically be generated by increasing degrees of partial melting (e.g. Mysen & Kushiro, 1977; Dick & Bullen, 1984; Nicolas, 1989). However, it is difficult to see how the chromitite bands within many of the dykes could have formed in this manner. In addition, the harzburgites, dunite dykes and dunite envelopes around chromitite pods all show notable LREE enrichment (Fig. 6), and the reaction-zone dunites have chondrite-normalized REE patterns indistinguishable from that of harzburgite sample L22 (Fig. 6b). The LREE/MREE ratios of these rocks are far too high for them to be solely the residuum of partial melting of MORB-source mantle (e.g. Prinzhofer & Allègre, 1985; McDonough & Frey, 1989). Such REE patterns of peridotites in the Trinity ophiolite were explained as the product of contamination by assimilated continental crustal material (Gruau *et al.*, 1998), Other processes include a mantle origin involving disequilibrium mechanisms (Prinzhofer & Allègre, 1985), the effect of melt transportation (Navon & Stolper, 1987) and the entrapment of small melt fractions (Song & Frey, 1989). On the other hand, LREE-enriched, U-shaped REE patterns of peridotites in the Oman ophiolite are explained as the product of interaction of the peridotites with LREE-enriched melts (Godard *et al.*, 2000; Takazawa *et al.*, 2003).

The podiform chromitites, which have dunite envelopes very similar in composition to the dunite dykes, consist of high-Cr magnesiochromite with Cr-numbers of 80–84, indicating crystallization from suprasubduction zone boninitic melts. Boninitic melts are characterized by U-shaped chondrite-normalized REE patterns similar to those observed in the reaction-zone dunites of Luobusa. Reaction of the Luobusa peridotites with such a melt could easily explain the observed LREE enrichment in

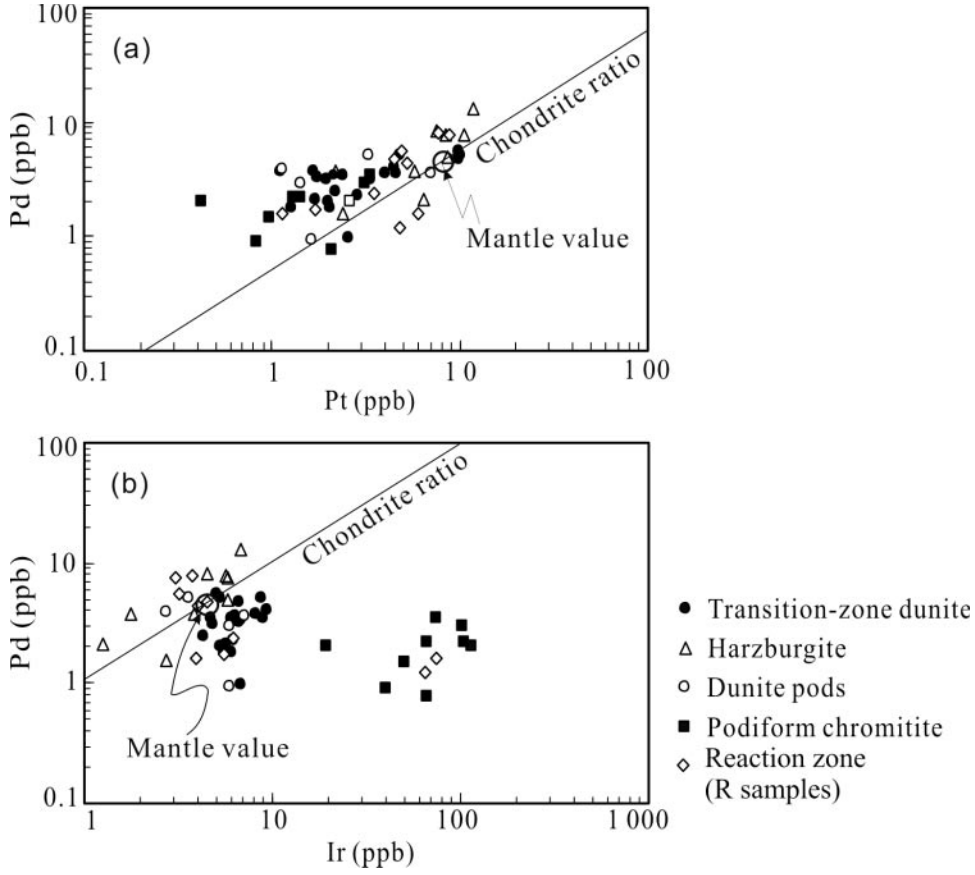

Fig. 8. Plots of (a) Pt versus Pd and (b) Ir versus Pd of the chromitites and dunites in the transition zone of the Luobusa ophiolite. Chondritic ratio (line) and mantle value are from Barnes *et al.* (1995).

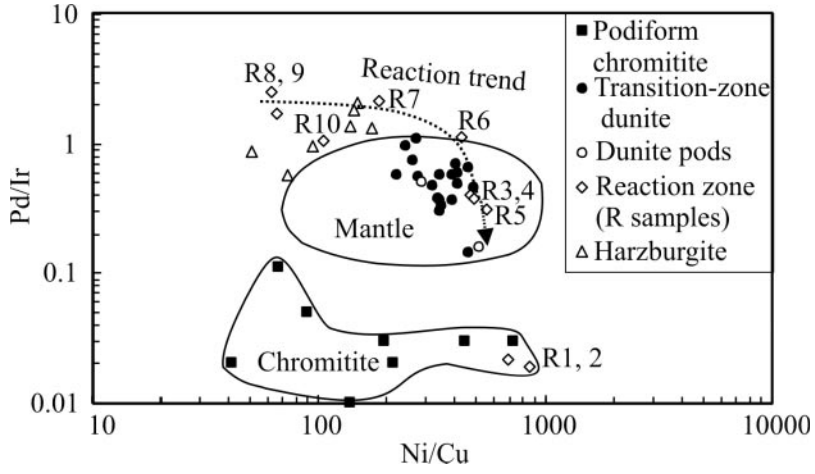

Fig. 9. Plot of Pd/Ir versus Ni/Cu for the podiform chromitites from the Luobusa ophiolite, compared with transition zone dunites, harzburgites and reaction zone samples. Referenced field of mantle is from Barnes *et al.* (1987).

the dunites. The reaction-zone dunites have marked positive Eu anomalies and several of the adjacent harzburgite samples have similar but less pronounced anomalies (Fig. 6e). These anomalies are compatible with melt impregnation leading to crystallization of trace amounts of microscopic to sub-microscopic plagioclase.

The chromitite forms a distinct band with sharp boundaries near the centre of the dyke, whereas the

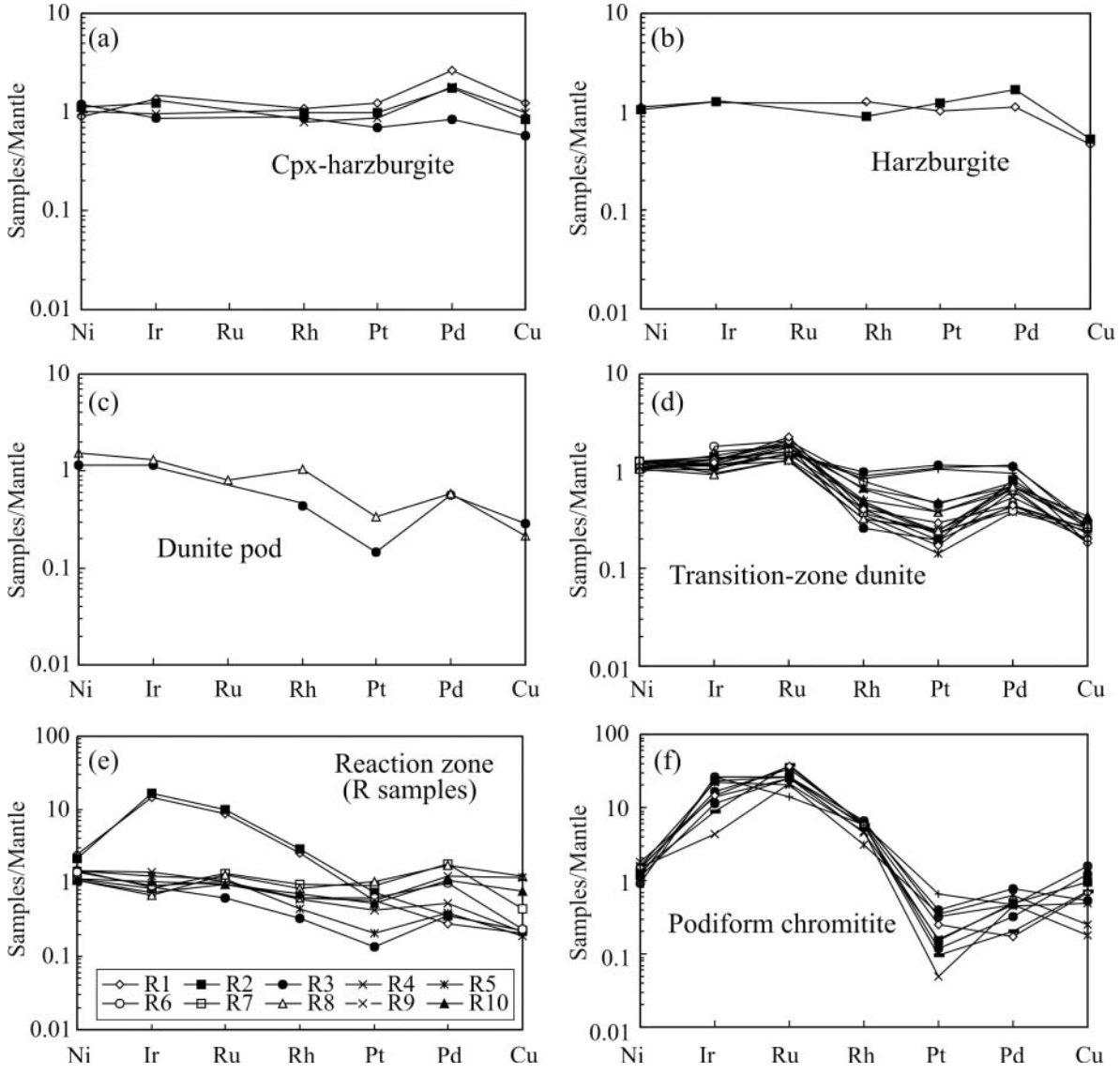

Fig. 10. Mantle-normalized Ni, PGE and Cu patterns of the chromitites and transition-zone dunites from the Luobusa ophiolite. The normalization values are Ni 2000 ppm, Ir 4·4 ppb, Ru 5·6 ppb, Rh 1·6 ppb, Pt 8·3 ppb, Pd 4·4 ppb and Cu 28 ppm (Barnes *et al.*, 1987).

dyke margins are gradational with the host harzburgite. This morphology supports the suggested origin of the dyke by melt–rock interaction rather than injection of ultramafic magma into a fracture and subsequent cooling and crystallization, which would more probably have resulted in sharp, well-defined dyke margins.

Melt–rock interaction in Luobusa has been postulated previously to explain the formation of podiform chromitites and their dunite envelopes (Zhou *et al.*, 1996). This process involves incongruent melting of orthopyroxene and precipitation of olivine (orthopyroxene = olivine + SiO_2-rich melt), thereby reducing or removing pyroxenes from the host cpx-bearing peridotites to form more depleted harzburgites and dunites, both of which are enriched in LREE and other incompatible elements. The transitional boundaries between the dunites and harzburgites (Fig. 2b) and the presence of interstitial relatively Ti-rich clinopyroxene in these rocks strongly support their formation by melt–rock interaction.

Processes involved in the formation of the Luobusa mantle sequence

The cpx-bearing harzburgites in Luobusa have generally higher Al, Ca, Zn, Cu and V and lower Mg-number than the more depleted harzburgites and dunites. They are characterized by relatively iron-rich olivine (Fo_{90}),

aluminous chromite (Cr-number as low as 20) and aluminous pyroxene (Zhou *et al.*, 1996)—features typical of relatively fertile abyssal peridotites (Dick & Bullen, 1984; Arai, 1994). Their chondrite-normalized REE patterns are moderately enriched in HREE and only weakly enriched in LREE. The chemistry and mineralogy of the cpx-bearing peridotites attest to their weakly depleted character, and they are interpreted as the residuum remaining after extraction of a MORB-like magma from a fertile mantle source (Zhou *et al.*, 1996).

Harzburgites have traditionally been viewed as depleted, refractory residues produced by partial melting of lherzolites and cpx-bearing harzburgites (Coleman, 1977). However, this interpretation does not account for the occurrence of harzburgites, such as those in the Luobusa ophiolite, that have well-developed, U-shaped REE patterns indicating significant LREE enrichment. Such patterns are now believed to reflect partial melting coupled with melt–peridotite interaction (Edwards, 1990; Bodinier *et al.*, 1991; Kelemen *et al.*, 1992; Suhr *et al.*, 1998). The depleted harzburgites, which make up the bulk of the Luobusa ophiolite, all have well-developed, U-shaped REE patterns, with or without small positive Eu anomalies. These patterns are nearly identical to those of the reaction-zone dunites in Luobusa (Fig. 5e), which were clearly formed by melt–rock reaction.

Relationships between Ni and Cu in the harzburgites and cpx-bearing harzburgites are consistent with Cu being an incompatible and Ni a compatible element. Cu decreases whereas Ni increases in the peridotites during melt–rock interaction (Fig. 7, R samples) because as sulphide is removed, the proportion of chalcopyrite in the sulphide decreases (Lorand *et al.*, 1993) and the modal proportion of olivine increases. This trend is very similar to the observed Cu–Ni variations in the Luobusa harzburgites, suggesting that the latter are also a result of melt–rock interaction.

The harzburgites have REE patterns similar to those of harzburgites in the Bay of Islands ophiolite, which have been interpreted as the products of metasomatic reaction between hydrous melts and depleted peridotite (Edwards & Malpas, 1995). Thus, comparison with other ophiolitic harzburgites and evidence from the dunite–harzburgite reaction zone strongly suggest that the harzburgites of Luobusa owe their composition to melt–rock interaction.

Transition-zone dunites, by definition, lie at the crust–mantle boundary, bracketed between tectonized peridotites below and layered cumulates above. Early studies, such as those by Coleman (1977), Greenbaum (1977) and Malpas (1978), suggested that the dunites are cumulate in origin and that they define a petrologic Moho within the transition zone. Later studies have suggested that transition-zone dunites may also be formed by high degrees of partial melting and/or by extensive melt–rock reaction. In Luobusa, the transition zone at the top of the mantle section consists of massive dunites, which are chemically homogeneous. Their coarse-grained character, extensive high-temperature deformation (Fig. 3) and highly magnesian character argue against an origin as magma chamber cumulates. In other ophiolites, however, such as the Bay of Islands, the transition-zone dunites commonly show cumulate textures in their upper parts and grade into layered troctolites and olivine gabbros that are clearly of crustal origin (Malpas, 1978). If such cumulate textures once existed in the Luobusa dunites, they have been obliterated by extensive deformation and recrystallization. The transition-zone dunites in Luobusa are petrographically similar to dunite envelopes around the chromitite pods and to the dunite dykes. All of the dunites have highly refractory olivine ($Fo_{89–93}$) with well-developed kink-banding and both contain minor orthopyroxene and interstitial clinopyroxene. They also have euhedral chromite grains with similar compositions that are relatively enriched in TiO_2 compared with those in the harzburgites. In addition, the transition-zone dunites all have well-developed, U-shaped, chondrite-normalized REE patterns similar to those of the dunite dykes, pods and envelopes (Fig. 6). In fact, the REE patterns of the transition-zone dunites are indistinguishable from those of the harzburgites and the dunite dyke. Some of the transition-zone dunites have small Eu anomalies identical to those of the dunite dyke and some of the harzburgites. The geochemical similarities between the transition-zone dunites and those clearly formed by melt–rock reaction in the dunite dyke provide strong evidence that the transition-zone dunites also formed by percolation of melts through the mantle section.

In mantle peridotites, PGE of the Ir-subgroup occur both as alloys (Os–Ir–Ru) and sulphides, whereas Pd and Pt are mainly associated with interstitial sulphide in the fertile mantle (lherzolite) (Mitchell & Keays, 1981). Reaction of the Luobusa mantle peridotites with S-undersaturated boninitic melts would have removed sulphides and left a dunite relatively enriched in Os, Ir and Ru, but depleted in Pt and Pd (Fig. 10). On the other hand, Pd would concentrate preferentially into the liquid, whereas Pt would form an alloy with iron (Fe–Pt), resulting in fractionation of Pt and Pd. Pt/Pd ratios would increase as melt–rock interaction progressed as seen in Luobusa. The negative correlation between Pd/Ir and Ni/Cu ratios (Fig. 9) suggests that Pd behaves like Cu and was removed, whereas Ir behaves like Ni and was retained during melt–rock interaction.

Geochemical constraints on melt compositions in the Luobusa ophiolite

MORB magmas have chondrite-normalized REE patterns depleted in LREE and, thus, are unlikely to have

been the type of melt that reacted with the Luobusa peridotites to form the U-shaped REE patterns of the peridotites and dunites. The depletion in MREE of the dunites and peridotites supports the interpretation that the migrating melts were themselves already strongly depleted in MREE. Boninites have chondrite-normalized, U-shaped REE patterns (e.g. Crawford *et al.*, 1989), similar to those observed in the Luobusa peridotites, suggesting that the passage of boninitic melts through the upper mantle produced the observed LREE-enriched mantle peridotites and dunites in Luobusa. Zhou *et al.* (1996, 1998) showed that the high-Cr podiform chromitites in Luobusa crystallized from boninitic melts and that these melts reacted with the surrounding harzburgites to form the dunite envelopes. Additional evidence for the presence of boninitic melts includes low-Al pyroxenes in these rocks (Table 2; Fig. 4), and the Cu and Ni contents of the dunites. Both the transition-zone dunites and the dunite dykes (samples R3, 4, 5, 6 in Fig. 7) in Luobusa have low Cu and high Ni contents, suggesting that the melt was S-undersaturated and was able to remove sulphide from the host rocks. The Cu depletion therefore supports the identification of a boninitic melt, because boninitic magmas are known to be S-undersaturated (Keays, 1995).

Percolation of similar boninitic melts through the Bay of Islands mantle sequence has been invoked to explain the formation of large refractory dunite bodies in that ophiolite (Edwards & Malpas, 1995; Suhr *et al.*, 1998, 2003).

Implications for the evolution of the Luobusa ophiolite

There are three distinct occurrences of dunites in Luobusa: dunite dykes in the cpx-bearing harzburgites along the southern margin of the ophiolite, dunites associated with podiform chromitites in depleted harzburgites and massive dunites in the transition zone (Fig. 1). The relationships between the shapes of the dunite bodies, the mineral compositional variations and the whole-rock compositional trends reflect the history of melt supply and deformation in the Luobusa peridotite (Fig. 11).

Dunite dykes in Luobusa are scattered through the host cpx-bearing peridotites that form the base of the reconstructed section, suggesting that the host harzburgite reacted only locally with boninitic melts, probably along cracks. The presence of chromitite bands in many of these dykes indicates that the magmas became chrome saturated during a late stage of melt evolution.

The podiform chromitites with dunite envelopes are distributed along a belt in the mantle sequence just below the transition-zone dunites. Harzburgite in this zone is more depleted than the cpx-bearing harzburgite along the southern margin of the ophiolite (Fig. 1). The chromitites with layered, massive, nodular, disseminated and brecciated textures are essentially chromite–olivine cumulates formed by crystallization of small pockets of melt (Robinson *et al.*, 1997). The harzburgites and dunites associated with the podiform chromitites are both enriched in LREE, suggesting extensive modification by the passage of boninitic melts (Fig. 11).

In Luobusa, the transition-zone dunites are petrographically, mineralogically and geochemically similar to dunites clearly formed by melt–rock interaction and thus are believed to have originated in a similar manner. The question remains, however, whether melt–rock interaction was the only process involved in formation of the Luobusa dunites. The presence of cumulate textures in some transition-zone dunites elsewhere (e.g. Greenbaum, 1977; Malpas, 1978) suggests that at least the upper portion of the transition zone may have been cumulate in origin. However, if such textures once existed in Luobusa, they have been destroyed by extensive deformation and recrystallization. Likewise, some of the dunites may reflect high degrees of partial melting during the first stage of ophiolite formation. This would be compatible with the upward change from cpx-bearing harzburgite to harzburgite to dunite that is observed in the Luobusa mantle sequence. However, any geochemical evidence of this process has also been overprinted by reaction with the later-stage boninitic melts.

A model is proposed to explain the formation for the Luobusa ophiolite (Fig. 11). At *c.* 126 Ma, an intra-oceanic subduction zone developed, such that the Luobusa peridotites represent a fragment of Neo-Tethyan oceanic lithosphere trapped in the mantle wedge above this subduction zone (Zhou *et al.*, 1996; Malpas *et al.*, 2003). Melting of the subducted slab and overlying mantle wedge produced hydrous boninitic melts, which were then injected into the Luobusa peridotites along cracks and fractures. These boninitic melts were out of equilibrium with the surrounding peridotite, leading to dissolution of pyroxene and precipitation of olivine. As the melts migrated upward through the mantle section, they were modified by melt–rock interaction. The Mg-number of olivine and Cr-number of chromite in the resulting rocks increased as the melt fraction increased by incongruent melting. When these melts reached the upper part of the mantle sequence, they ponded in small pockets, where they continued to react with the host harzburgite, increasing the silica contents of the melts and leading to precipitation of chromitite pods with dunite envelopes. The podiform chromitites lie at a relatively uniform depth within the mantle, suggesting that the rising melts ponded at the point where mantle flow changed from vertical to subhorizontal (Fig. 11). The ponded melts infiltrated the host harzburgites, leading to precipitation of Ti-rich chromite and to modification of the bulk-rock chemistry.

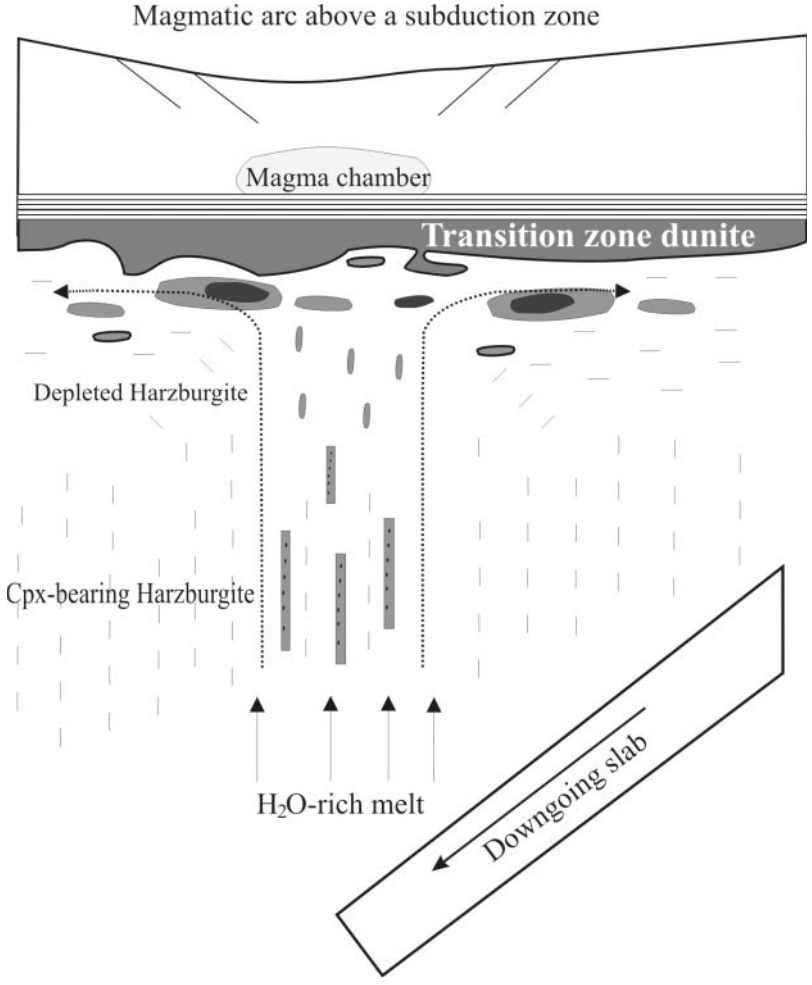

Fig. 11. A possible petrogenetic model for the formation of the Luobusa mantle sequence. Cpx-bearing harzburgite formed at a mid-ocean spreading centre is trapped in a mantle wedge above a subduction zone. Fluids released from the downgoing slab lead to the formation of boninitic melts in a fore-arc region. Passage of these melts through the harzburgite leads to melting out of pyroxene to form depleted harzburgite in the upper parts of the section. Ponding of the melts at the point where mantle flow changed from vertical to horizontal led to extensive melt–rock reaction and to precipitation of podiform chromitites surrounded by dunite envelopes. Further rise of the melts caused complete removal of pyroxenes from the harzburgite and the formation of the transition-zone dunites. Fractionation of the remaining melts in a crustal magma chamber may have contributed some cumulate dunite to the top of the transition zone.

The host harzburgites, even those away from the podiform chromitites, show evidence of LREE enrichment by the infiltrating melts. Finally, melts from which olivine and chromite had been extracted migrated upward into the (pre-existing?) transition zone, where they ponded at the top of the mantle. Continued reaction with the host rocks removed any remaining pyroxene to form the massive dunites, which also show LREE enrichment.

A mantle wedge above a subduction zone is an ideal site in which to generate boninitic melts (e.g. Plank & Langmuir, 1998) and the geochemistry of volcanic rocks in the Dagzhuka ophiolite, located in the same suture zone about 200 km west of Luobusa, is compatible with an arc-related environment (Xia *et al.*, 2003). Fluid inclusions in olivine and chromite indicate that the Luobusa chromitites were formed from hydrous melts (Bai *et al.*, 2000).

A hydrous environment is also required to form podiform chromitites as seen in Luobusa (Bai *et al.*, 2000; Edwards *et al.*, 2002) and as experimentally documented (Matveev & Ballhaus, 2002). Water is known to be present in mantle wedges above subduction zones because peridotite xenoliths from such regions commonly contain hydrous minerals, such as amphibole (Takahashi, 1986). Melting of orthopyroxene in harzburgite to produce dunite, as described above, requires both relatively high temperatures (1100°C) and the presence of water.

As discussed above, the cpx-bearing harzburgite (= relatively fertile harzburgite) in Luobusa may originally have been an abyssal peridotite, but the chromitites,

depleted harzburgites and dunites formed in a different tectonic setting. The high Cr-numbers of the chromite in these rocks (up to 84) are similar to those in fore-arc peridotites (Dick & Bullen, 1984; Pearce *et al.*, 1984; Arai, 1994). This tectonic setting is favourable for producing boninitic melts (e.g. Crawford *et al.*, 1989), which were essential for the formation of the podiform chromitites in Luobusa.

SUMMARY AND CONLUSIONS

Dunites in the mantle sequence of the Luobusa ophiolite show geochemical and mineralogical evidence of formation primarily by melt–rock interaction in the upper mantle in a suprasubduction zone environment. Cpx-bearing harzburgites that formed originally by moderate degrees of partial melting at a mid-ocean spreading ridge were variably modified later by hydrous boninitic melts. Deep in the section, dunite dykes formed within relatively weakly modified cpx-bearing harzburgites where melt/rock ratios were small and passage of the boninite melt was fast. At higher levels, pods of chromitite and dunite bodies mark a zone in which the mantle flow changed from vertical to subhorizontal and where extraction of melt was less efficient. The ponded melts reacted with the host peridotites such that the SiO_2 contents of the melts increased, leading to precipitation of the podiform chromitites. The remaining melt continued to migrate upward to the crust–mantle boundary, where pervasive melt–rock interaction led to formation of the massive transition-zone dunites. At all stages of this process, melt–rock interaction dissolved Pd- and Pt-bearing sulphide from the host harzburgite, leaving Pd- and Pt-depleted dunites.

Comparison with other ophiolites suggests that the transition-zone dunites in Luobusa may have formed by a combination of crystal fractionation, high degrees of partial melting and extensive melt–rock interaction. The uppermost transition-zone dunites may originally have formed by crystal fractionation from crustal magma chambers during the first stage of evolution, whereas the lowest ones may reflect high degrees of partial melting. However, evidence of these processes, if once present, has been obliterated by invasion of the boninitic melts. If this interpretation is correct, the previous identification of a 'petrologic Moho' at the base of the transition zone and a 'seismic Moho' at the base of the cumulate section (Greenbaum, 1977; Malpas, 1978) needs to be reconsidered. It seems more likely that the crust–mantle boundary lies somewhere within the transition zone, which is formed by a combination of mantle and crustal processes. The dominant process may vary from ophiolite to ophiolite. In Luobusa, the present transition zone reflects predominantly mantle processes but some ophiolites still preserve evidence of crustal processes as well.

ACKNOWLEDGEMENTS

This study was supported by grants from the Research Grant Council of Hong Kong SAR, China (HKU7086/01P to J.M. and HKU7101/01P to M.F.Z) and the Natural Sciences and Engineering Research Council of Canada (NSERC) to P.T.R. Fieldwork was logistically supported by local geological teams of the Tibetan Geological Survey. Careful reviews by Dr N. T. Arndt, Dr J.-L. Bodinier and an anonymous reviewer resulted in significant improvement of this paper and are gratefully acknowledged.

REFERENCES

Aitchison, J. C., Badengzhu, Davis, A. M., Liu, J. B., Luo, H., Malpas, J. G., *et al.* (2000). Remnants of a Cretaceous intra-oceanic subduction system within the Yarlung–Zangbo suture (southern Tibet). *Earth and Planetary Science Letters* **183**, 231–244.

Aitchison, J. C., Badengzhu, Davis, A. M. & Luo, H. (2003). The Gangdese thrust: a phantom structure that did not raise Tibet. *Terra Nova* **15**, 155–162.

Arai, S. (1980). Dunite–harzburgite–chromitite complexes as refractory residue in the Sangun–Yamaguchi zone, Western Japan. *Journal of Petrology* **21**, 141–165.

Arai, S. (1994). Characterization of spinel peridotites by olivine–spinel compositional relationships: review and interpretation. *Chemical Geology* **113**, 191–204.

Bai, W.-J., Zhou, M.-F., Robinson, P. T., Fang, Q., Yan, B., Zhang, Z., *et al.* (2000). *Origin of podiform chromitites, diamonds and associated mineral assemblage in the Luobusa ophiolite, Southern Tibet.* Beijing: Seismological Press, 98 pp.

Barnes, S.-J., Naldrett, A. J. & Gorton, M. (1985). The origin of the fractionation of platinum-group elements in terrestrial magmas. *Chemical Geology* **53**, 303–323.

Barnes, S.-J., Boyd, R., Korneliussen, A., Nilsson, L.-P., Often, M., Pedersen, R. B., *et al.* (1987). The use of mantle normalization and metal ratios in discriminating between the effects of partial melting, crystal fractionation and sulphide segregation on platinum-group elements, gold, nickel and copper: examples from Norway. In: Prichard, H. M., Potts, P. J., Bowles, J. F. W. & Cribb, S. J. (eds) *Geo-Platinum Symposium Volume.* London: Elsevier, pp. 113–143.

Bodinier, J.-L., Menzies, M. A. & Thirlwall, M. F. (1991). Continental to oceanic mantle transition: REE and Sr–Nd isotopic geochemistry of the Lanzo lherzolite massif. *Journal of Petrology special volume 'Orogenic Lherzolites and Mantle Processes'*, 191–210.

Buchl, A., Brugmann, G., Batanova, V. G., Munker, C. & Hofmann, A. W. (2002). Melt percolation monitored by Os isotopes and HSE abundances: a case study from the mantle section of the Troodos Ophiolite. *Earth and Planetary Science Letters* **204**, 385–402.

Coleman, R. G. (1977). *Ophiolites: Ancient Oceanic Lithosphere.* Berlin Springer, 229 pp.

Crawford, A. J., Falloon, T. J. & Green, T. H. (1989). Classification, petrogenesis and tectonic setting of boninites. In: Crawford, A. J. (ed.) *Boninites and Related Rocks.* London: Unwin Hyman, pp. 1–49.

Dick, H. J. B. & Bullen, T. (1984). Chromian spinel as a petrogenetic indicator in abyssal and alpine-type peridotites and spatially associated lavas. *Contributions to Mineralogy and Petrology* **86**, 54–76.

Dick, H. J. B. & Natland, J. H. (1996). Late stage melt evolution and transport in the shallow mantle beneath the East Pacific Rise: Deep Sea Drilling Project. *Initial Reports* **147**, 103–134.

Edwards, S. J. (1990). Harzburgites and refractory melts in the Lewis Hills massif, Bay of Island ophiolite complex: the base-metals and precious-metals story. *Canadian Mineralogist* **28**, 537–552.

Edwards, S. J. & Malpas, J. (1995). Multiple origins for mantle harzburgites: examples from Lewis Hills, Bay of Islands ophiolite, Newfoundland. *Canadian Journal of Earth Sciences* **32**, 1046–1057.

Edwards, S. J. & Malpas, J. (1996). Melt–peridotite interactions in shallow mantle at the East Pacific Rise: evidence from ODP Site 895 (Hess Deep). *Mineralogical Magazine* **60**, 191–206.

Edwards, S. J., Pearce, J. A. & Freeman, J. (2002). New insights concerning the influence of water during the formation of podiform chromitite. In: Dilek, Y., Moores, E., Elthon, D. & Nicolas, A. (eds) *Ophiolites and Oceanic Crust: New Insights from Field Studies and the Ocean Drilling Program. Geological Society of America, Special Paper* **349**, 139–147.

Eggins, S. M., Woodhead, J. D. & Kinsley, L. P. J. (1997). A simple method for the precise determination of ≥40 trace elements in geological samples by ICP–MS using enriched isotope internal standardization. *Chemical Geology* **134**, 311–326.

Godard, M., Jousselin, D. & Bodinier, J.-L. (2000). Relationships between geochemistry and structure beneath a palaeo-spreading centre: a study of the mantle section in the Oman ophiolite. *Earth and Planetary Science Letters* **180**, 133–148.

Greenbaum, D. (1977). The chromitiferous rocks of the Troodos ophiolite complex. *Economic Geology* **72**, 1175–1194.

Gruau, G., Bernard-Griffiths, J. & Lecuyer, C. (1998). The origin of U-shaped rare earth patterns in ophiolite peridotites: assessing the role of secondary alteration and melt/rock reaction. *Geochimica et Cosmochimica Acta* **62**, 3545–3560.

Jain, J. C., Field, M. P. & Neal, C. R. (2000). Determination of the REE in geological reference materials DTS-1 (dunite) and PCC 1 (peridotite) by ultrasonic and microconcentric desolvating nebulisation ICP–MS. *Geostandards Newsletter* **24**, 65–72.

Keays, R. R. (1995). The role of komatiitic and picritic magmatism and S-saturation in the formation of the ore deposits. *Lithos* **34**, 1–18.

Kelemen, P. B., Dick, H. J. B. & Quick, J. E. (1992). Formation of harzburgite by pervasive melt/rock reaction in the upper mantle. *Nature* **358**, 635–641.

Kelemen, P. B., Shimizu, N. & Salters, V. J. M. (1995). Extraction of mid-ocean-ridge basalt from the upwelling mantle by focused flow of melt in dunite channels. *Nature* **375**, 747–753.

Kubo, K. (2002). Dunite formation processes in highly depleted peridotite: case study of the Iwanaidake Peridotite, Hokkaido, Japan. *Journal of Petrology* **43**, 423–448.

Kushiro, I., Yoder, H. S. & Nishikawa, M. (1968). Effect of water on the melting of enstatite. *Geological Society of America Bulletin* **79**, 1685–1692.

Lorand, J. P., Keays, R. R. & Bodinier, J.-L. (1993). Copper- and noble-metal enrichment across the lithospheric–asthenospheric boundary of mantle diapirs: evidence from the Lanzo lherzolite massif. *Journal of Petrology* **34**, 1111–1140.

Malpas, J. (1978). Magma generation in upper mantle, field evidence from ophiolite suites, and application to generation of oceanic lithosphere. *Philosophical Transactions of the Royal Society of London, Series A* **288**, 527–545.

Malpas, J., Zhou, M.-F., Robinson, P. T. & Reynolds, P. (2003). Geochemical and geochronological constraints on the origin and emplacement of the Yarlung–Zangbo ophiolites, Southern Tibet. In: Dilek, Y. & Robinson, P. T. (eds), *Ophiolites Through Earth History. Geological Society, London, Special Publications* **218**, 191–206.

Matveev, S. & Ballhaus, C. (2002). Role of water in the origin of podiform chromitite deposits. *Earth and Planetary Science Letters* **203**, 235–243.

McDonough, W. F. & Frey, F. A. (1989). Rare earth elements in upper mantle rocks. In: Lipin, B. R. & McKay, G. A. (eds) *Geochemistry and Mineralogy of Rare Earth Elements. Mineralogical Society of America Reviews in Mineralogy* **21**, 99–145.

Mitchell, R. H. & Keays, R. R. (1981). Abundance and distribution of gold, palladium and iridium in some spinel and garnet lherzolites: implications for the nature and origin of precious metal-rich intergranular components in the upper mantle. *Geochimica et Cosmochimica Acta* **45**, 2425–2442.

Mysen, B. & Kushiro, I. (1977). Compositional variations of coexisting phases with degree of melting of peridotite in the upper mantle. *American Mineralogist* **62**, 843–865.

Navon, O. & Stolper, E. (1987). Geochemical consequences of melt percolation: the upper mantle as a chromatographic column. *Journal of Geology* **95**, 285–307.

Nicolas, A. (1989). *Structures of Ophiolites and Dynamics of Oceanic Lithosphere*. Dordrecht: Kluwer Academic, 367 pp.

Nicolas, A. & Prinzhofer, A. (1983). Cumulative or residual origin for the transition zones in ophiolites, structural evidence. *Journal of Petrology* **24**, 188–206.

Olive, V., Ellam, R. M. & Wilson, L. (2001). A protocol for the determination of the rare earth elements at picomole level in rocks by ICP–MS: results on geological reference materials USGS PCC 1 and DTS-1. *Geostandards Newsletter* **25**, 219–228.

Pallister, J. S. & Hopson, C. A. (1981). Samail ophiolite plutonic suite: field relations, phase variation, cryptic variation and layering, and a model of a spreading ridge magma chamber. *Journal of Geophysical Research* **86**, 2593–2644.

Parkinson, I. J. & Pearce, J. A. (1998). Peridotites from the Izu–Bonin–Mariana forearc (ODP Leg 125): evidence for mantle melting and melt–mantle interaction in a supra-subduction zone setting. *Journal of Petrology* **39**, 1577–1618.

Pearce, J. A., Lippard, S. J. & Roberts, S. (1984). Characteristics and tectonic significance of suprasubduction zone ophiolites. In: Kokelaar, B. P. & Howells, M. F. (eds) *Marginal Basin Geology. Geological Society, London, Special Publications* **16**, 77–94.

Plank, T. & Langmuir, C. H. (1998). The chemical compositions of subducting sediments and its consequences for the crust and mantle. *Chemical Geology* **145**, 325–394.

Potts, P. J., Thompson, M. & Chenery, S. R. N. (2003). GeoPT 12: an international proficiency test for analytical geochemistry laboratory-report on Round 12 (GAS Serpentinite).

Prichard, H. M. & Lord, R. A. (1993). An overview of the PGE concentrations in the Shetland ophiolite complex. In: Prichard, H. M., Alabaster, T., Harris, N. B. W. & Neary, C. R. (eds) *Magmatic Processes and Plate Tectonics. Geological Society, London, Special Publications* **76**, 273–294.

Prinzhofer, A. & Allègre, C. J. (1985). Residual peridotites and the mechanisms of partial melting. *Earth and Planetary Science Letters* **74**, 251–265.

Proenza, J., Gervilla, F., Melgarejo, J. C. & Bodinier, J. L. (1999). Al- and Cr-rich chromitite from the Mayari–Baracoa ophiolite belt (Eastern Cuba): consequence of interaction between volatile-rich melts and peridotites in suprasubduction mantle. *Economic Geology* **94**, 547–566.

Qi, L., Zhou, M.-F., Malpas, J. & Sun, M. (2004). Determination of the REEs in ultramafic rocks by inductively coupled plasma mass spectrometry after preconcentration of REE using $Fe(OH)_3$ and $Mg(OH)_2$ coprecipitation. *Geostandards Newsletter* (in press).

Quick, J. E. (1981). The origin and significance of large, tabular dunite bodies in the Trinity peridotite, Northern California. *Contributions to Mineralogy and Petrology* **78**, 413–422.

Robinson, P. T., Zhou, M.-F., Malpas, J. & Bai, W.-J. (1997). Podiform chromitites: their composition, origin and tectonic setting. *Episodes* **20**, 247–252.

Roeder, P. L., Campbell, I. H. & Jamieson, H. E. (1979). Re-evaluation of the olivine–spinel geothermometer. *Contributions to Mineralogy and Petrology* **68**, 325–334.

Song, Y. & Frey, F. A. (1989). Geochemistry of peridotite xenoliths in basalt from Hannuoba, Eastern China: implications for subcontinental mantle heterogeneity. *Geochimica et Cosmochimica Acta* **53**, 97–113.

Suen, C. J., Frey, F. A. & Malpas, J. (1979). Bay of Islands ophiolite suite, Newfoundland: petrologic and geochemical characteristics with emphasis on Rare Earth Element geochemistry. *Earth and Planetary Science Letters* **45**, 337–348.

Suhr, G., Seck, H. A., Shimizu, N. & Gunther, D. (1998). Infiltration of refractory melts into the lowermost oceanic crust: evidence from dunite- and gabbro-hosted clinopyroxenes in the Bay of Islands ophiolite. *Contributions to Mineralogy and Petrology* **131**, 136–154.

Suhr, G., Hellebrand, E., Snow, J. E., Seck, H. A. & Hofmann, A. W. (2003). Significance of large, refractory dunite bodies in the upper mantle of the Bay of Islands Ophiolite. *Geochemistry, Geophysics, Geosystems* **4**, Article No. 8605.

Sun, Y.-L., Zhou, M.-F. & Sun, M. (2001). Routine Os analysis by isotope dilution-inductively coupled plasma mass spectrometry: OsO_4 in water solution gives high sensitivity. *Journal of Analytical Atomic Spectrometry* **16**, 345–349.

Takahashi, E. (1986). Genesis of calc-alkali andesite magma in a hydrous mantle crust boundary: petrology of lherzolite xenoliths from the Ichinomegata Crater, Oga Peninsula, Northeast Japan. *Journal of Volcanology and Geothermal Research* **29**, 355–395.

Takazawa, E., Okayasu, T. & Satoh, K. (2003). Geochemistry and origin of the basal lherzolites from the northern Oman ophiolite (northern Fizh block). *Geochemistry, Geophysics, Geosystems* **4**, Article No. 1021.

Xia, B., Yu, H. X., Chen, G. W., Qi, L., Zhao, T. P. & Zhou, M.-F. (2003). Geochemistry and tectonic environment of the Dagzhuka ophiolite in the Yarlung–Zangbo suture zone, Tibet. *Geochemical Journal* **37**, 311–324.

Zhou, M.-F. (1995). Petrogenesis of the podiform chromitites in the Luobusa ophiolites, Southern Tibet. Ph.D. thesis, Dalhousie University, Canada.

Zhou, M.-F., Robinson, P. T., Malpas, J. & Li, Z. (1996). Podiform chromitites in the Luobusa ophiolite (Southern Tibet): implications for melt–rock interaction and chromite segregation in the upper mantle. *Journal of Petrology* **37**, 3–21.

Zhou, M.-F., Sun, M., Keays, R. R. & Kerrich, R. (1998). Controls on platinum-group elemental distributions of podiform chromitites: a case study of high-Cr and high-Al chromitites from Chinese orogenic belts. *Geochimica et Cosmochimica Acta* **62**, 677–688.

Zhou, M.-F., Yumul, G. P., Jr, Malpas, J. & Sun, M. (2000). Comparative study of platinum-group elements in the Acoje and Coto Blocks of the Zambales ophiolite, Philippines. *The Island Arc* **9**, 556–564.

Zhou, S., Mo, X. X., Mahoney, J. J., Zhang, S. Q., Guo, T. J. & Zhao, Z. D. (2002). Geochronology and Nd and Pb isotope characteristics of gabbro dykes in the Luobusa ophiolite, Tibet. *Chinese Science Bulletin* **47**, 143–146.